Scaturro, P., Stukalov, A., Haas, D. A., Cortese, M., Draganova, K., Plaszczyca, A., et al. (2018). An orthogonal proteomic survey uncovers novel Zika virus host factors. Nature, 561(7722), 253-257. doi:10.1038/s41586-018-0484-5.

DOI: 10.1038/s41586-018-0484-5

URL: https://www.nature.com/articles/s41586-018-0484-5

An Orthogonal Proteomic Screen of Zika virus Reveals Specific Targeting of Neuronal Differentiation Factors.

Pietro Scaturro[1,2], Alexey Stukalov[1,2], Darya A. Haas[1], Mirko Cortese[3], Kalina Draganova[4], Anna Płaszczyca[3], Ralf Bartenschlager[3,6], Magdalena Götz[4] and Andreas Pichlmair[1,2,5]

[1]Max-Planck Institute of Biochemistry, Innate Immunity Laboratory; Am Klopferspitz 18, 82152 Martinsried, Germany

[2]Technical University of Munich, School of Medicine, Institute of Virology, Munich, Germany,

[3]Department of Infectious Diseases, Molecular Virology, University of Heidelberg, 69120 Heidelberg, Germany

[4]Institute for Stem Cell Research, Helmholtz Center Munich, German Research Center for Environmental Health, 85764 Neuherberg, Germany; Physiological Genomics Physiological Genomics and SYNERGY, Excellence Cluster for Systems Neurology, Biomedical Center, Ludwig-Maximilian University Munich, 82152 Planegg/Munich, Germany;

[5]German Center for Infection Research (DZIF), Munich partner site, Germany

[6]German Center for Infection Research (DZIF), Heidelberg partner site, Germany

Address correspondence to:

Andreas Pichlmair - Technical University Munich, Institute of Virology; Schneckenburger str. 8, 81675 Munich, Germany

e-mail address: andreas.pichlmair@tum.de

Abstract

Zika virus (ZIKV) has recently emerged as a global health concern due to its widespread diffusion and its association with severe neurological symptoms and microcephaly in newborns[1]. However, the molecular mechanisms responsible for ZIKV pathogenicity remain largely elusive. Here, we used human neural progenitor cells (hNPC) and the neuronal cell line SK-N-BE2 in an integrated proteomics approach to characterize cellular responses to viral infection on proteome and phosphoproteome level as well as affinity proteomics to identify cellular targets of ZIKV proteins. This approach identified 386 ZIKV-interacting proteins, unraveling ZIKV-specific and pan-flaviviral activities as well as host factors with known functions in neuronal development, retinal defects and infertility. Moreover, our analysis identified 1,216 phosphosites specifically up- or down-regulated upon ZIKV infection, indicating profound modulation of fundamental signaling pathways such as AKT, MAPK/ERK and ATM/ATR providing mechanistic insights into the proliferation arrest elicited by ZIKV infection. Functionally, our integrative study identifies previously unexplored ZIKV host-dependency factors, providing a comprehensive framework for a system-level understanding of ZIKV-induced perturbations at the protein and cellular pathway levels.

Main text

ZIKV, a Flavivirus related to Dengue (DENV), West-Nile (WNV) and Hepatitis C virus (HCV), has a single stranded RNA genome of positive polarity, encoding for a polyprotein that is co- and post-translationally processed into three structural (capsid, prM, and envelope) and seven nonstructural proteins (NS1-NS2A-NS2B-NS3-NS4A-NS4B-NS5)[2]. To comprehensively understand how ZIKV targets and affects neuronal cells, we performed an unbiased proteome survey to identify cellular proteins and associated complexes interacting with each of the ten ZIKV proteins (isolated from the clinical Asian isolate FSS13025[3]) expressed in a human neuroblastoma cell line (SK-N-BE2) (Fig. 1a, Extended Data Fig. 1a). Given the complex membrane topology of the polyprotein, we designed each of the viral expression constructs to undergo appropriate polypeptide processing and correct insertion into the ER membrane (Extended Data Fig. 1a). Except for NS2A, all ZIKV proteins were correctly expressed and processed (Extended Data Fig. 1b-c). Specificity controls included NS4B of HCV (NS4B-HCV) and *Gaussia luciferase*. One-step affinity

purification coupled with Liquid chromatography and Mass spectrometry (AP-LC-MS/MS) followed by Bayesian statistical modelling, allowed to identify 386 proteins specifically associating with ZIKV open-reading frames (ORFs), resulting in 484 high-confident interactions (Fig. 1b, Extended Data Fig. 2 and Supplementary Table 1). We identified a high number of previously reported *bona fide* interactors of flavivirus proteins, validating the dataset. ZIKV-NS4B, for instance, associates with several subunits of the ATPase (ATP1A1, 1A2, 1A3, 1B and 6V1H), voltage-dependent anion selective channel proteins (VDAC1,2,3) and calcium-binding mitochondrial proteins (i.e. SLC25A, SLC38A1) as well as components of the cytochrome C oxidase complex (COX15, MT-CO2, NDUFA4), confirming ATP production, calcium homeostasis, apoptosis, and mitochondrial respiratory chain, as important targets of diverse flaviviruses[4] (Extended Data Fig. 2). Similarly, mining the Capsid cellular interactome revealed nuclear and nucleolar-resident proteins such as nucleolin (NCL), nucleolar RNA-dependent helicases of the DDX family, core histones (H2A) as well as peroxisomal proteins including PEX19 that have previously been reported as cellular targets of DENV and WNV (Fig. 1b and Extended Data Fig. 2)[5-7]. Most importantly, this analysis uncovered host factors not previously associated with flaviviruses and enriched in ER-, mitochondria- and nuclear-resident proteins largely reflecting the subcellular localization of the viral protein (Extended Data Fig. 2). Furthermore, this dataset revealed a number of proteins linked to neurological diseases or development, particularly among the Capsid- and NS4B-specific interactors (Fig. 1b). For instance, among the Capsid interactors were LARP7 (involved in telomere stability and mutated in Alazami syndrome)[8], LYAR (important for maintenance of embryonic stem cells identity)[9] and NGDN (a neuronal development factor)[10] (Ext Data Fig. 4b). Of particular interest are interactors of NS4B, one of the vORFs recently suggested to be involved in inhibition of neuronal development via activation of autophagy[11]. In direct comparison with HCV-NS4B, ZIKV-NS4B showed specific enrichment in cellular proteins covering functions associated with the whole spectrum of ZIKV-associated pathogenesis ranging from neurodegenerative disorders and retinal degeneration (CLN6, BSG), to regulators of neuronal differentiation (CEND1, RBFOX2) and axonal dysfunction (CHP1, TMEM41b) (Fig. 1b, Extended Data Fig. 2, 3). Ablation or natural mutations of these proteins drive neurological disorders, confirming their roles in neuronal development[12-17]. Co-immunoprecipitation followed by western blotting (Co-IP) verified that these proteins specifically associate with arthropod-borne NS4Bs (such as DENV and ZIKV) and not

NS4B of other flaviviruses such as HCV; with a subset of proteins specifically binding only to ZIKV-NS4B (TMEM41b, CEND1, CLN6; Fig. 2a). Furthermore, reciprocal Co-IP also confirmed NS4B association in ZIKV-infected cells (Extended Data Fig. 4a). ZIKV-NS4B precipitated particularly well Ceroid-lipofuscinosis neuronal protein 6 (CLN6), which is associated with a lysosomal storage disease causing neurodegenerative late-infantile disorders as well as retinal defects[12] (Fig. 2b and Extended Data Fig. 4a). Sub-cellular localization analysis of ZIKV-infected or NS4B-transduced primary hNPC indicated profound redistribution of CLN6 to sites of viral replication and NS4B, respectively (Figure 4c, d and Extended Data Fig. 4d). AP-LC-MS/MS experiments using CLN6 as bait pinpointed binding partners shared between NS4B and CLN6 (Extended Data Fig. 4e), such as SLC7A5 (also known as LAT1) – a neutral amino acids transporter functioning at the brain blood barrier with involvement in neurogenesis and retina homeostasis[18]. Furthermore, CLN6 associated specifically with mTOR and TELO2, important regulators of signaling pathways that have been reported to be affected by ZIKV infection[11,19]. Altogether, the ZIKV-vORF interactome in human neuronal cells revealed a multitude of new Flavivirus host binding partners, including cellular proteins and signalling pathways components involved in neuronal development.

In patients, during early stages of development, ZIKV predominantly infects neural progenitor cells[20,21] causing microcephaly and other neurodevelopmental injuries. In order to gain insights into ZIKV-induced perturbations occurring at the onset of brain development we employed a human induced pluripotent stem cell-derived neuronal differentiation model. In the first step we defined the global proteomic changes occurring during differentiation of hNPC into neurons[22] using LC-MS/MS analysis (Extended Data Fig. 5a, b). Importantly, markers of neuronal differentiation such as βIII-tubulin (TUBB3), microtubule-associated proteins 2 and 6 (MAP2, MAP6), neuronal cell adhesion molecule 1 (NCAM1), doublecortin (DCX) and ELAV-Like RNA Binding Protein 3 (ELAVL3) (Fig. 2c, Supplementary Table 2) were significantly upregulated, corroborating the progression of hNPC towards neuronal differentiation. Next, we investigated the influence of ectopic expression of ZIKV-NS4B and HCV-NS4B on early neuronal differentiation. Notably, ectopic expression of ZIKV-NS4B, but not of HCV-NS4B, during differentiation specifically altered the expression of a subset of proteins, many of which particularly relevant for neuronal development (Fig. 2e and Extended Data Fig. 5c-d, Supplementary Table 3). For example, a subset of

factors involved in neuronal differentiation (e.g. MAP2, -6, DPYSL3, -5, CNTN2; Fig. 2d, green squares and circles) as well as proteins associated with neurological diseases, including DOK3[23] and SUMO2[24], were downregulated in ZIKV-NS4B but not HCV-NS4B transduced cells (Fig. 2d,e, Extended Data Fig. 5c and Supplementary Table 2). These observations suggest that ZIKV-NS4B perturbs specific developmental programs. Similar effects could be seen in proteomic analysis of hNPC infected with ZIKV in the presence or absence of differentiation stimuli (Extended Data Fig. 6a). ZIKV infection led to a general antiviral response evinced by robust up-regulation of type-I interferon stimulated genes (e.g. STAT1, MX1, OAS3, IFIT1 etc.). However, infection also led to specific down-regulation of neuronal factors under differentiation conditions (Extended Data Fig. 6b and Supplementary Table 4). Altogether, these experiments unveil for the first time the distinct proteomic signatures of ZIKV and ZIKV-NS4B on differentiating hNPC, revealing specific targets deregulated during neurogenesis.

Growing evidence suggests that protein post-translational modifications, especially phosphorylation, play a crucial role in controlling and executing the complex and dynamic reorganization of signal-transduction pathways upon infections by a broad range of viruses[25-29]. We therefore used time-resolved phosphoproteomics[30] to investigate cellular pathway dysregulation upon ZIKV infection. SK-N-BE2-infected or mock-treated cells were harvested 24, 48 and 72 hours post ZIKV infection and their phosphoproteome was quantitatively analyzed by label-free LC-MS/MS. This analysis identified 14,222 unique phosphosites (localization probability ≥ 0.75; Extended Data Fig. 7a-d), 1,216 of which were modulated upon ZIKV infection (Fig. 3a and Supplementary Table 5). Analysis of biological functions enriched among the sites specifically affected by ZIKV infection revealed cellular assembly and organization, cell-cycle regulation, as well as nervous system (NS) development and neurological diseases as significantly modulated (Fig. 3b, Supplementary Table 6). Most importantly, the depth of details achieved by this approach allowed us to map specific phosphorylation events along entire cellular pathways highlighting modulation of key processes such as ATM, AKT/mTOR and ERK/MAPK signaling cascades (Fig. 3c-g, Extended Data Fig. 7, Supplementary Tables 7-8). For instance, we could identify profound down-regulation of the AKT-mTOR signaling pathway, as indicated by de-phosphorylation of known AKT1 substrates (e.g. DNMT1, TBC1D4, LARP6), mTOR targets (e.g. ANKRD17, LARP1, PATL1, EEF2K), the central kinase S6K and its main effector protein S6. Coherently with down-regulation of the

AKT-mTOR signaling pathway, we also found increased phosphorylation of proteins, such as the negative regulator of autophagy DAP, at residues known to inhibit its suppressor effect and consistent with the notion that autophagy is induced after ZIKV infection[11,31] (Fig. 3d,g, Extended Data Fig. 7f). Interestingly, ZIKV infection additionally down-regulated the MAPK/ERK-signaling pathway, since both A-RAF and ERK2 as well as several substrates of the downstream ERK1/2 Map kinases (EIF4EBP1, BAZ1B, TWIST) were significantly de-phosphorylated upon ZIKV infection (Fig. 3c, Supplementary Tables 5, 8). While modulation of autophagy or the AKT/mTOR pathway has been recently associated with ZIKV[11], our data now allow to quantitatively map individual phosphorylated residues onto signalling pathways on a global scale. In this respect, complex crosstalks between different cellular pathways modulated upon ZIKV infection could be identified (Extended Data Fig. 7e). For instance, both ERK1/2 and mTOR pathways converge on S6K and modulate its phosphorylation status[32] (Fig. 3c), suggesting multiple possible mechanisms contributing to the observed ZIKV-induced upregulation of autophagy, diminished hNPC proliferation and impaired neurogenesis. Noteworthy, we could also observe a massive up-regulation of the ATM (ataxia-telangiectasia mutated)/ATR (ATM- and Rad3-Related) DNA-damage pathway, as inferred from significantly increased phosphorylation of several substrates of ATR (NPM1, CGGBP, GINS2), DNAPK (XRCC4) and downstream effector proteins (H2AFX) as well as proteins involved in cell cycle regulation and DNA damage checkpoint (TOP2B, CDK1) (Supplementary Tables 5, 8). Our data therefore suggest a mechanistic link between the observed ZIKV-induced cell-cycle arrest[19] and p53 activation[33], since persistent activation of DNA damage repair pathways in response to ZIKV-induced mitotic abnormalities (such as multipolar spindle and supernumerary foci[19]) might lead to cell death of neuronal progenitors (Fig. 3c). Most importantly, this analysis sheds light on previously unreported ZIKV targets with known functions in neurogenesis. Among these, we noted prominent dephosphorylation of proteins such as p38 MAPK and downstream targets (HSP27 and ATF7), MARCKS (one of the main PKC substrates) and DPYSL2, whose activation positively modulates neurite outgrowth and brain development (Fig. 3f-g)[34-38].

To assess the functional relevance of the host factors newly identified through our orthogonal proteomic survey, we selected cellular targets regulated either at the proteome (n=26), phosphoproteome (n=8) or interactome (n=21) level by ZIKV. Expression of individual proteins was silenced by shRNA and the

consequences on virus infection were determined by plaque assay (Fig. 4a, Extended Data Fig. 8a-c and Supplementary Table 10). This approach identified 17 host-factors whose silencing significantly reduced ZIKV replication as compared to NT controls (Fig. 4a). Besides confirming the essential role for recently described cellular factors in ZIKV replication, such as STT3A[39], MGGT1[40] and MSI1[41], we identified 14 additional host proteins critically required for ZIKV replication. Among these were proteins whose cellular abundance was strongly decreased upon NS4B expression and/or ZIKV infection in differentiating hNPC cells (i.e. DOK3, XIRP2, YIPF4 and LMOD3), proteins that changed phosphorylation status upon ZIKV infection (LMO7, FXR1 and LARP7) and ZIKV interacting proteins (i.e. Capsid: LARP7 and LYAR; NS4B: BSG and CLN6) (Fig. 4a). Importantly, validation experiments confirmed that CEND1, CLN6, CHP1, LMOD3, TMEM41b and BSG knockdown resulted in inhibition of ZIKV replication (Fig. 4b, and Extended Data Figure 8d, e, f). Moreover, infection of hNPC with two different ZIKV isolates (H/PF/2013 and MR766) recruited CLN6 and TMEM41b to sites enriched in dsRNA and NS4B, further corroborating their involvement in viral replication (Fig. 4c, d, e).

In this orthogonal proteomic survey we combined quantitative information at the proteome, phosphoproteome and interactome levels with publicly available interaction databases in order to get a holistic perspective on ZIKV impact in neuronal cells (Extended Data Fig. 9, Supplementary Table 9). Our integrated dataset offers the opportunity to pinpoint relationships between cellular proteins that are specifically exploited by ZIKV, and allows deducing potential driving mechanisms responsible for neurotoxicity. The interactome suggests entry points of hijacked signaling pathways, which could be tracked by phosphoproteome changes, while long-term effects accumulate on the proteome level. For instance, this orthogonal intersection revealed putative novel links between ZIKV-NS4B and activation of DNA damage and mTOR signaling pathways, as exemplified by the identification of CLN6 among the NS4B-specific interactors (Fig. 4f). Additionally, these data can be used to infer hotspots targeted by ZIKV at multiple levels. For example, the ZIKV host factor LARP7, is a Capsid-specific interactor that is additionally hypophosphorylated by ZIKV. Similarly, LMO7 is simultaneously downregulated at the protein level and hyperphosphorylated upon virus infection (Fig. 4f).

In general, our data provide valuable insights into how ZIKV exerts its action on candidate proteins previously identified in high-throughput genetic as well as drug-based screens. For instance, a recently published FDA-approved drug screen identified among the ZIKV inhibitors Digoxin, an inhibitor of the ATP1A1 Na2+/K+, here identified as NS4B-specific interactor. Fingolimod is an inhibitor of the Sphingosine1 phosphate receptor – S1PR2, which is persistently hypophosphorylated upon ZIKV-infection. Finally, Mycophenolic Acid/MPA, an inhibitor of the Inosine-5-monophosphate dehydrogenase 1 – IMPDH1 was identified as specifically down-regulated protein in ZIKV infected cells[42]. A CRISPR-based screen for ZIKV identified STT3A, an Oligosaccharyltransferase complex subunit, and SSR3, the Translocon-associated protein subunit gamma, as important ZIKV host-dependency factors. Both proteins are identified here as cellular binders of NS2B-3 and NS4B[39]. Although some of the ZIKV binding partners identified here may associate with orthologues of closely related flaviviruses (e.g. DENV, WNV), their role in ZIKV-related pathogenesis might in addition rely on the unique ability of ZIKV to cross the placental barrier and reach the developing brain[43].

Our study suggests that ZIKV evolved multiple mechanisms to usurp, exploit or perturb fundamental cellular processes, ultimately contributing to the broad spectrum of pathological abnormalities observed in humans. In addition, this study provides a rationale resource for streamlining ZIKV-research efforts and considering or excluding intracellular pathways for specific therapeutic intervention.

Methods

Cell lines and reagents

HeLa S3 (CCL-2.2) and Vero E6 cells (CRL-1586) were purchased from ATCC. SK-N-BE2 cells were kindly provided by Rüdiger Klein (MPI of Neurobiology, Munich). HEK293 cells were a gift from Andrew Bowie (Trinity College, Dublin). Human Neural Progenitor (hNPC) cells were generated as described below. All cell lines were tested to be mycoplasma free and their identity verified by STR profiling. Primary antibodies used in this study were: rabbit polyclonal anti-CEND1 (1:5000 WB, #ab113076; Abcam), rabbit polyclonal anti-RBFOX2 (1:500 WB, #HPA006240; Sigma-Aldrich), rabbit polyclonal anti-CLN6 (1:500 WB, #SAB4502281; Sigma-Aldrich), rabbit polyclonal anti-CHP1 (1:500 WB; #PA5-29876; Thermo-Fisher), rabbit polyclonal anti-BSG (1:2000 WB, #HPA036048; Sigma-Aldrich), rabbit polyclonal anti-TMEM41b (1:250 WB, #HPA014946; Sigma-Aldrich), mouse monoclonal anti-dsRNA J2 (1:400 IFA; Scicons), mouse IgG2bκ anti-HA (1:500 IFA; 12CA5; Sigma-Aldrich), rabbit polyclonal anti-DENV NS4B (1:100 IFA; 1:500 WB; #GTX124250; Genetex. This antibody cross-reacts with ZIKV-NS4B, as validated by immunodetection of ZIKV-NS4B in cells transduced with HA-tagged NS4B or ZIKV-infected cell lysates (Extended Data Fig. 4b)). For detection of NS4B and Capsid upon ZIKV infection by western-blotting, the rabbit polyclonal anti-ZIKV NS4B and anti-ZIKV Capsid (1:1000 WB, #GTX133311; and 1:1000, #GTX133317 Genetex) were used. For detection of phosphorylated and total protein abundance by WB, mouse monoclonal anti-gammaH2Ax (#ab22551; Abcam) and the following rabbit monoclonal antibodies were used (Cell Signalling Technology): anti-MARCKS (#D88D11) and anti-phospho-MARCKS (#D13E4), rabbit monoclonal anti-mTOR (#7C10) and anti-phospho-mTOR (#D9C2), p38-MAPK (#D13E1) and anti-phospho-p38 MAPK (#D3F9), S6 ribosomal protein (#5G10) and anti-phospho S6 (#D57.2.2E). Where indicated, to increase the basal phosphorylation of certain cellular proteins, 12-O-tetra-decanoylphorbol-13-acetate (TPA, Cell Signalling Technologies) or DMSO, were added to the culture medium (32 nM) 15 minutes before harvesting cell lysates for WB analysis. For characterization of hNPC by immunofluorescence, the following antibodies were used: mouse anti-GFAP (#G3893; Sigma-Aldrich), rat anti-Ki67 (#14-5698; EBioscience), mouse anti-MAP2 (#M4403, clone HM-2; Sigma-Aldrich), mouse anti-Nestin (#MAB5326, clone 10C2; Millipore), rabbit anti-Sox2 (#ab137385, Abcam).

Generation, maintenance and differentiation of human neural progenitor cells (hNPCs)

Human induced pluripotent stem cells (iPSC) generated from healthy patient fibroblasts were maintained in mTeSRTM 1 media (STEMCELL Technologies) on Geltrex (ThermoFischer Scientific) plates in the absence of feeders. The iPSC were regularly confirmed to be mycoplasma-negative. The protocol used for derivation of human neural progenitor cells (hNPC) has been previously described[44] with modifications. Briefly, iPSC colonies were harvested with a cell scraper to ensure relatively big colonies remain and cultured in suspension to form embroid bodies (EBs) in DMEM/F-12, 0.5% N2 supplement (Gibco), 5µM Dorsomorphin (Sigma-Aldrich), 10µM SB431542 (Sigma-Aldrich) and 10 µM Rho-associated kinase inhibitor (ROCK) (Y-27632, StemCell Technologies). EB were grown for 5 days with media changed every other day before gentle trituration and attachment on poly-ornithine/laminin coated dishes in NPC media consisting of DMEM/F-12, 0.5% N2, 1% B27 supplement with 10 ng/ml bFGF (Peprotech 100-18B-50) and 10 µM ROCK. Three to four days after EB plating, neural rosettes were manually isolated, dissociated mechanically to single cells and plated on fresh poly-ornithine/laminin coated dishes in NPC media with 10 µM ROCK inhibitor. On the next day, the media was changed to NPC media without ROCK and NPCs were propagated for up to 12 passages by splitting with accutase when 70-80% confluency was reached. For short-term differentiation experiments (Fig. 3c, d, e and Extended Data Fig. 4), $2x10^5$ cells were seeded on 6-well plates, transduced with empty lentiviruses (NT), lentiviruses expressing HCV- or ZIKV-NS4B or infected with 0.01 MOI of ZIKV H/PF/2013. Forty-height hours later differentiation was induced for 5 days by growth factor withdrawal and addition of 10 µM ROCK inhibitor, while undifferentiated cells were kept in NPC media in the presence of bFGF. In both cases media was replaced every other day. Cell pellets were harvested, snap-frozen and processed for LC-MS/MS analysis as described below.

Virus strains, virus stocks preparation and generation of lentiviruses

ZIKV strains H/PF/2013 and MR766 were obtained from the European Virus Archive (EVAg, France). Virus stocks were passaged once on VeroE6 cells and virus-containing cell culture supernatants or conditioned medium from uninfected cells were harvested from day 3 to 8 post-infection. Supernatants were filtered through a 0.45 µM pore-size filter and stored at -70 °C. Titers of infectious virus were

determined by plaque assay as previously described (see below). For infection of hNPCs, virus stocks were diluted in hNPC medium and cells were inoculated for 2 h at 37°C. Inocula were removed and fresh hNPC medium (basal or differentiation) was added. Mock cells were inoculated with equal amounts of conditioned medium.

For generation of lentiviruses expressing the individual HA-tagged ZIKV viral proteins or FLAG-tagged host proteins, synthetic cDNAs (sequences based on recently described recombinant ZIKV strain FSS13025, Asian lineage[3]) were obtained in pUDC57 vectors and the fusion gene inserted into the lentiviral pWPI expression plasmid. Lentivirus expressing the HA-tagged NS4B of Hepatitis C virus was previously described[45]. Lentivirus stocks were produced and titrated as described[4]. Nucleotide sequences of each construct are available upon request.

Lentiviral shRNA Library Production and shRNA screen

From the MISSION TRC lentiviral library (Sigma-Aldrich), 54 MS hits and 4 controls were selected and shRNA were produced as follows. Two different shRNA-expressing lentiviruses per gene (116 shRNAs in total; Supplementary Table 10) were produced individually in HEK 293T cells ($8x10^5$) that were plated one day prior to transfection. Transfections were performed as previously described[4] using packaging plasmids psPAX2 and pMD-VSV-G (kindly provided by Dr. Didier Trono) and shRNA-encoding pLKO-puro plasmids. Viruses were collected at 48 and 72h post-transfection, clarified by centrifugation and pooled prior to freezing. Controls included non-targeting shRNA-encoding plasmid SHC001 and SHC002 (NT1 and NT2) as well as known virus restriction factors ATP6V0C and Musashi1. For quality control purposes, approximately 25% of random samples were used to measure lentiviral titers. For screening purposes, 10,000 SK-N-BE2 cells per well were seeded in 96-well plates in 90 µl of complete DMEM and 24 hours later cells were transduced with 30ul of each lentivirus (MOI≈3) in triplicate wells/replica and three independent biological replicates). Three days later cells were infected with 0.1 MOI of ZIKV H/PF/2013, and 48 h.p.i. cell supernatants were used for titration by PFU assay. Cell Viability was measured by a Resazurin-based cell-viability assay, on plates which were transduced with shRNAs in parallel but were not ZIKV-infected. In brief, 50 µg/ml resazurin was added to each well of a 96-well plate and incubated for 30 min at 37 °C, followed by measurement of fluorescence (535/590 nm) using an

Infinite 200 PRO series micro plate reader (Tecan). The normalization for the virus titers and fluorescence measurements were performed in 2 steps. First, the measurements in each replicate experiment were adjusted by the median factor of the replicate (the median of $X_{g,i}$/median($X_{g,1}$, $X_{g,2}$, $X_{g,3}$) across all the shRNAs (g=1,2,...,116), where $X_{g,i}$ is the titer of g-th shRNA in i-th replicate). Then the adjusted measurements were normalized, such that the average signal of Non-targeting controls was 100%. The following criteria were applied to select hits: ≥50% decrease in median viral titers with two shRNAs or ≥75% if only one shRNA was efficient; cell viability ≥75% of NT controls. Validation experiments on selected shRNAs (Fig.4b, and Ext Data Figure 8c-d) were performed on 24-well plates using the same overall protocol.

Virus titration by plaque assay

Confluent monolayers of VeroE6 cells were infected with serial 10-fold dilutions of virus supernatants for 2 h at 37 °C. Inoculum was removed and replaced with serum-free MEM (Gibco, Life Technologies) containing 1.5% carboxymethylcellulose (Sigma-Aldrich). Four days post-infection, cells were fixed for 2 h at room temperature with formaldehyde directly added to the medium to a final concentration of 5%. Fixed cells were washed extensively with water before being stained with H_2O containing 1% crystal violet and 10% ethanol for 30 min. After rinsing with water, the number of plaques was counted and virus titers were calculated.

Deep proteomes and phosphoproteome sample preparation

For proteomic and phosphoproteomic analysis, SK-N-BE2 cells (10^7 cells/biological replicate/condition; 4 biological replicates/condition), were mock-infected or infected with ZIKV H/PF/2013 at an MOI of 3. Cell pellets were harvested after 24, 48 and 72 hours, lysed in 1mL of lysis buffer (10 mM Tris-HCl [pH 7.5], 4% SDS, and 0.05 mM DTT supplemented with complete protease and phosphatase inhibitor cocktails [Roche]), boiled 10' at 98 °C, and sonicated (4°C for 15 min, or until a homogeneous suspension was formed). Clarified protein lysates were precipitated with acetone, and normalized protein mixtures resuspended in 500 µL TFE digestion buffer. Protein digestion was performed by adding 1:100 (protein:enzyme) trypsin and LysC with rapid agitation (2,000 rpm) overnight at 37°C. An aliquot of the

peptide mixtures was used for determination of the total proteome (10%) as previously described[46] while the remaining peptide mixture (90%) was processed for phosphopeptide enrichment using the EasyPhos protocol[30]. For proteomic analysis of primary cells, hNPC were seeded in 6-well plates ($2x10^5$ cells/well) and either mock-infected, infected with 0.01 MOI of ZIKV or transduced with lentiviruses expressing HA-tagged ZIKV-NS4B or HCV-NS4B (MOI=3). Two days after infection or lentivirus transduction, cells were left in hNPC proliferation media (undiff.) or neuronal differentiation was initiated by culturing the cells in hNPC differentiation media (diff.). Five days later cell pellets were collected and processed for label-free LC-MS/MS analysis as described before[46]. Each condition was performed in quadruplicate biological replicates.

Deep proteome and phosphoproteome LC-MS/MS analysis and data processing

Peptide mixtures were separated on a 50 cm reversed-phase column (diameter of 75 µm packed in-house with ReproSil-Pur C18-AQ 1.9 µm resin [Dr. Maisch GmbH]) as previously described[47].

Raw MS files were processed within the MaxQuant environment (version 1.5.7) using the integrated Andromeda search engine with FDR ≤ 0.01 at the protein, peptide, and modification level. Proteome and phosphoproteome files were assigned to separate search parameter groups. The search included fixed modifications for carbamidomethyl (C) and variable modifications for oxidized methionine (M), acetylation (protein N-term), and phospho (STY) for phosphoproteome files. Peptides with at least six amino acids were considered for identification, and “match between runs” was enabled with a matching time window of 0.7 min to transfer MS1 identifications between runs. Peptides and proteins were identified using a UniProt FASTA database from human (UniprotKB release 2015_08 including isoforms and unreviewed sequences) and ZIKV virus polyprotein corresponding to the H/PF/2013 strain (NCBI GenBank KJ776791.2; individual viral cleavage products were manually annotated).

Sample preparation for affinity-purification of ZIKV proteins and cellular proteins

For the determination of the ZIKV interactome, four independent affinity purifications were performed for each ZIKV HA-tagged viral protein. SK-N-BE2 cells were transduced with an MOI of 3 of each lentivirus ($8x10^6$ cells/dish) and 72 hours later cells were scraped in 1 ml of Lysis Buffer (50 mM Tris pH=8, 150 mM

NaCl, 0.5% NP-40, cOmplete protease inhibitor cocktail, Roche) and HA-affinity purifications performed as described before[48]. Briefly, clarified cell lysates were incubate with anti-HA-specific beads for 3h at 4°C, and non-specifically bound proteins removed by three washes with Lysis buffer and 5 washes with Washing Buffer (50 mM Tris pH=8, 150 mM NaCl). Bound proteins were denatured by incubation in 20 µl Guanidinium Chloride buffer (600 mM GdmCl, 1mM TCEP, 4mM CAA, 100 mM Tris/HCl pH 8). After digestion with 1 µg LysC (WAKO Chemicals USA) at room temperature for 3 h, the suspension was diluted in 100 mM Tris/HCl (pH 8), and the protein solution was digested with trypsin (Promega) overnight at room temperature. Peptides were purified on stage tips with three C18 Empore filter discs (3M) and analyzed by mass spectrometry as described previously[49]. For the analysis of CLN6 and other host factors interactome, SK-N-BE2 cells were transduced with the corresponding FLAG-tagged lentiviruses and 72 hours later cell lysates were processed as described above, using agarose anti-FLAG M2 beads (Sigma-Aldrich).

Data processing of AP-LC-MS/MS samples

Raw mass-spectrometry data were processed with MaxQuant (software version 1.5.3) using the built-in Andromeda search engine to search against the human proteome (UniprotKB release 2015_08 including isoforms and unreviewed sequences) containing forward and reverse sequences plus ZIKV virus polyprotein (ZIKV strain FSS13025, Asian lineage[3] NCBI GenBank KU955593.1 with individual viral cleavage products manually annotated), Gaussia luciferase (Q9BLZ2), NS4B of Hepatitis C virus (E7ELX2) sequences, and the label-free quantitation algorithm as described previously[50]. In MaxQuant, carbamidomethylation was set as fixed and methionine oxidation and N-acetylation as variable modifications, using an initial mass tolerance of 6 ppm for the precursor ion and 0.5 Da for the fragment ions. Search results were filtered with a false discovery rate (FDR) of 0.01 for peptide and protein identifications.

Statistical analysis of MS data

MaxQuant output files (proteinGroups.txt and “Phospho (STY) Sites.txt” for proteome and phosphoproteome data, respectively) were processed by a combination of in-house R (version 3.3), Julia (version 0.5) and Stan (version 2.14) scripts.

To account for the variation in the analyzed biological sample amounts and MS performance, we have inferred the normalizing multipliers for each MS run so that the normalized LFQ values of the representative set of proteins (ca. 500 randomly selected from the ones quantified in most of the normalized samples) do not change between the samples. First, this procedure was applied to normalize replicate MS runs within each condition, and then the normalization multipliers were further adjusted to normalize the conditions between each other. For the analysis of proteome changes the LFQ intensities were fit to a generalized linear Bayesian statistical model for each protein group (raw intensities of each phosphosite for phosphoproteome data) individually. The model employed horseshoe priors for the model effects, and natural logarithm as a linking function for protein intensities. Additional parameters with horseshoe priors were introduced to model the biological variation within replicate samples. The MS measurements were set to follow Laplace distribution. Technical MS runs from both LTQ-Orbitrap XL and Orbitrap Q Exactive HF were used to estimate the signal-to-noise ratio and sensitivity of protein quantitation across the whole dynamic range of protein intensities. We used the obtained technical variation models to define the scale parameter of Laplace distribution for each individual MS measurement as well as scale and location parameters of the logistic distribution for missing MS measurements. The experimental design matrices and global horseshoe prior parameters for GLM models used to fit each individual data set were defined as follows (using R GLM formula language):

Data set	R GLM formula	τ_1 Horseshoe Prior Parameter for Model Effects	τ_2 Horseshoe Prior Parameter for Biological Variation
hNPC proteome	`log(intensity) ~ 1 + differentiation + treatment + differentiation:treatment`	1.0	0.25
SKN proteome and phosphoproteome	`log(intensity) ~ 1 + after_24h + after_48h + treatment + treatment:(after 24h + after 48h)`	2.0 (proteome) 1.0 (phosphosites)	0.1 (proteome) 0.25 (phosphosites)
ZIKV AP-LC-MS/MS	`log(intensity) ~ 1 + bait`	1.0	0.3
ZIKV host targets AP-LC-MS/MS	`log(intensity) ~ 1 + bait`	2.0	0.1

The posterior distributions of model parameters were inferred using Hamiltonian Markov Chain Monte Carlo (MCMC) method (Stan version 2.14), employing 8 parallel MCMC chains, 2000 warmup and 2000 sampling iterations taking every 4th sample from each chain. The statistical significance (*p*-value) of a hypothesis that given model variable *X* is positive, i.e. probability that a random sample of its posterior distribution would be non-positive ($P(X \leq 0)$), was calculated by approximating the posterior distribution from MCMC samples using Gaussian kernel with Silverman's rule-of-thumb bandwidth. For the $X \neq 0$ hypothesis the *p*-value was defined as $min(P(X \leq 0), P(X \geq 0))$. P-value ≤ 0.01 and |median (log_2 fold-change)| ≥ *1* criteria were used for reporting significantly regulated proteins and phosphosites (Supplementary Tables 2, 5 and 9).

To filter for specific AP-MS interactions, the inferred posterior distributions of protein intensities in each viral bait of ZIKV AP-MS dataset was compared with the average distribution of the same protein in all other baits excluding Capsid protein (due to its highly hydrophobic character and multiple subcellular localizations). The interaction was considered specific, if one-sided *p*-value (calculated as described above) was below 5×10^{-5} for Capsid bait (since there were no other baits with the same biochemical properties) and 5×10^{-2} for the other baits, and median protein enrichment against the background was more than 5.56-fold ($=2^{2.5}$) for high-confident and 2-fold for the lower-confidence set of ZIKV protein interactions. The same filtering strategy was applied to AP-MS experiments of selected host targets; the *p*-value cutoff was set 0.02 and log_2 Fold-change ≥1.5. For networks representation, sub-cellular localization of cellular proteins was extracted from Gene Ontology (Version 2016-Sep-21).

Datasets merging

The integration of all AP-MS, proteomic and phosphoproteomic data was done by matching protein groups of individual data sets to each other using in-house scripts. The protein groups were matched if they shared a common protein accession code ("Majority Protein ACs" column in MaxQuant output). In ambiguous situations (e.g. one protein group of dataset A shares different protein sequences with several protein groups of data set B) the priority was given to the reviewed protein sequences and canonical isoforms.

Integrating published protein-protein interactions, kinase-substrate relations and regulatory sites data

For overlaying our data with published protein-protein interactions we used IntAct interactions database (version 2017.04.08), IntAct complexes collection (version 2017.04.08) and CORUM protein complexes database (version 2017.03.15). The interaction (physical association) was included if both interacting partners were significantly enriched in the same ZIKV bait. For published AP-MS interactions we additionally required that one of the interacting partners was a bait. To integrate AP-MS datasets with proteomic and phosphoproteomic screens, only published direct interactions (including kinase–substrate relationships) were considered.

For phosphoproteomic analysis kinase-substrate relations and regulatory sites were extracted from PhosphositePlus[51] (kinase_substrate_dataset from Mar 21 2017 and regulatory_sites from Apr 18 2017, respectively).

Ingenuity pathway analysis

Proteome and phosphoproteome changes along with unchanged proteins or sites, respectively, were submitted to the IPA core analysis. The following cut-offs were set for differentially-expressed proteins: *p*-value ≤ 0.01 and $|\log_2$ (fold-change)$| \geq 1$. Ingenuity knowledge base was used as reference data-set, while only experimentally observed findings were used for confidence filtering. No filters were applied at the level of species, tissues or cell lines. Input datasets were used for the functional analysis to identify biological functions and canonical pathways that were most significant. Fisher's exact test was used to calculate *p*-values. Biological functions or pathways were considered significant for *p*-values ≤ 0.05.

Co-immunoprecipitation assays

For validation of ZIKV-NS4B interacting proteins, SK-N-BE2 cells were seeded into 15-cm^2 dishes ($8x10^6$ cells/dish), transduced with lentiviruses expressing ZIKV or HCV HA-tagged viral proteins or conditioned cell culture media. Seventy-two hours post-transduction, cell monolayers were scraped into 1 ml lysis buffer (50 mM Tris-HCl [pH 8.0], 0.5% NP-40, 150 mM NaCl and protease inhibitor cocktail (cOmplete, Roche), and clarified lysates processed for immunoprecipitation as described above. Eluted proteins were

further analyzed by western blot as specified in the figure legends. For reciprocal co-immunoprecipitation experiments, SK-N-BE2 cells were transduced with lentiviruses expressing each FLAG-tagged host protein and three days later infected with ZIKV at an MOI of 3. Seventy-two hours post-infection, cell monolayers were processed for immunoprecipitation with anti-FLAG M2 agarose beads (Sigma-Aldrich) as described above.

Immunofluorescence analysis

Human Neural progenitor cells (10^5 cells/well) seeded on poly-ornithine/laminin coated glass slides were transduced with lentiviruses (MOI=3) expressing FLAG-tagged proteins or empty control for 1h at 37°C. The next day media was changed and 48 h post-transduction cells were infected with ZIKV MR766 or H/PF/2013 at an MOI of 5 for 1h at 37°C. After 24h cells were fixed with 4% PFA, permeabilized with 0.1% (vol/vol) Triton X-100 in PBS and unspecific binding sites blocked with PBS containing 5% BSA for 1h at RT, and subjected to immunofluorescence staining using anti-FLAG antibody, anti-DENV NS4B or J2 anti-dsRNA. Secondary staining was performed with donkey anti-mouse Alexa568-conjugated and goat anti-rabbit Alexa 488-conjugated antibodies. Nuclear DNA was stained with 4′,6-diamidino-2-phenylindole (DAPI) (Molecular Probes). Coverslips were mounted in Fluoromount-G mounting medium (Southern Biotechnology Associates). Fluorescence images were acquired with a Leica SP8 inverted confocal microscope using a 63x Plan-Apo N.A. 1.4 objective. Image analysis was performed using FIJI (http://fiji.sc/wiki/index.php/Fiji)[52] and Pearson´s correlation coefficients were calculated using Coloc2 plugin.

Accession numbers

UniprotKB accession codes of all protein groups and proteins identified by Mass Spectrometry are provided in each respective Supplementary Table and were extracted from UniprotKB (Human; release 2015_08 including isoforms and unreviewed sequences). cDNA sequences corresponding to individual ZIKV open-reading frames used for generation of ZIKV lentivirus library (KU955593.1) or related to the wild-type ZIKV H/PF/2013 strain (KJ776791.2) were extracted from GenBank. Protein sequences of Gaussia luciferase (E7ELX2) and Hepatitis C virus NS4B (Q9BLZ2) were extracted from UniprotKB.

Data availability

The MS-based proteomics data were deposited at the ProteomeXchange Consortium (http://proteomecentral.proteomexchange.org) via the PRIDE partner repository with the data set identifier XXXXX [*raw mass-spectrometry files will be deposited on publicly accessible databases at a later stage*].

Author Contributions

P.S. and A.P. conceived the study. P.S. and D.A.H. performed most of the experiments. K.D. performed hNPC cell culture and characterization thereof, M.G. and R.B. intellectually contributed toward data interpretation. A.S. implemented the bioinformatic pipeline, statistical analysis and data integration. A.Pla. generated the samples used for phosphoproteomic analysis. M.C. generated and analyzed immunofluorescence stainings. P.S., A.S., D.A.H., M.G., R.B. and A.P. wrote the manuscript.

Acknowledgments

We thank Daniela Mauceri, Francesca Sacco, Laurent Chatel-Chaix and Martin Steger for helpful discussions and Renate Hornberger, Igor Paron, Korbinian Mayr and Gabriele Sowa for excellent technical assistance. The work in the authors' laboratory is funded by an ERC starting grant (StG 311339, iVIP), the Max-Planck free floater program, the German Research Foundation (PI1084/2-1, PI1084/3-1 and TRR179) and the Federal Ministry for Education and Research (ERA-Net grant ERASe).

Figures and Figure Legends

Figure 1

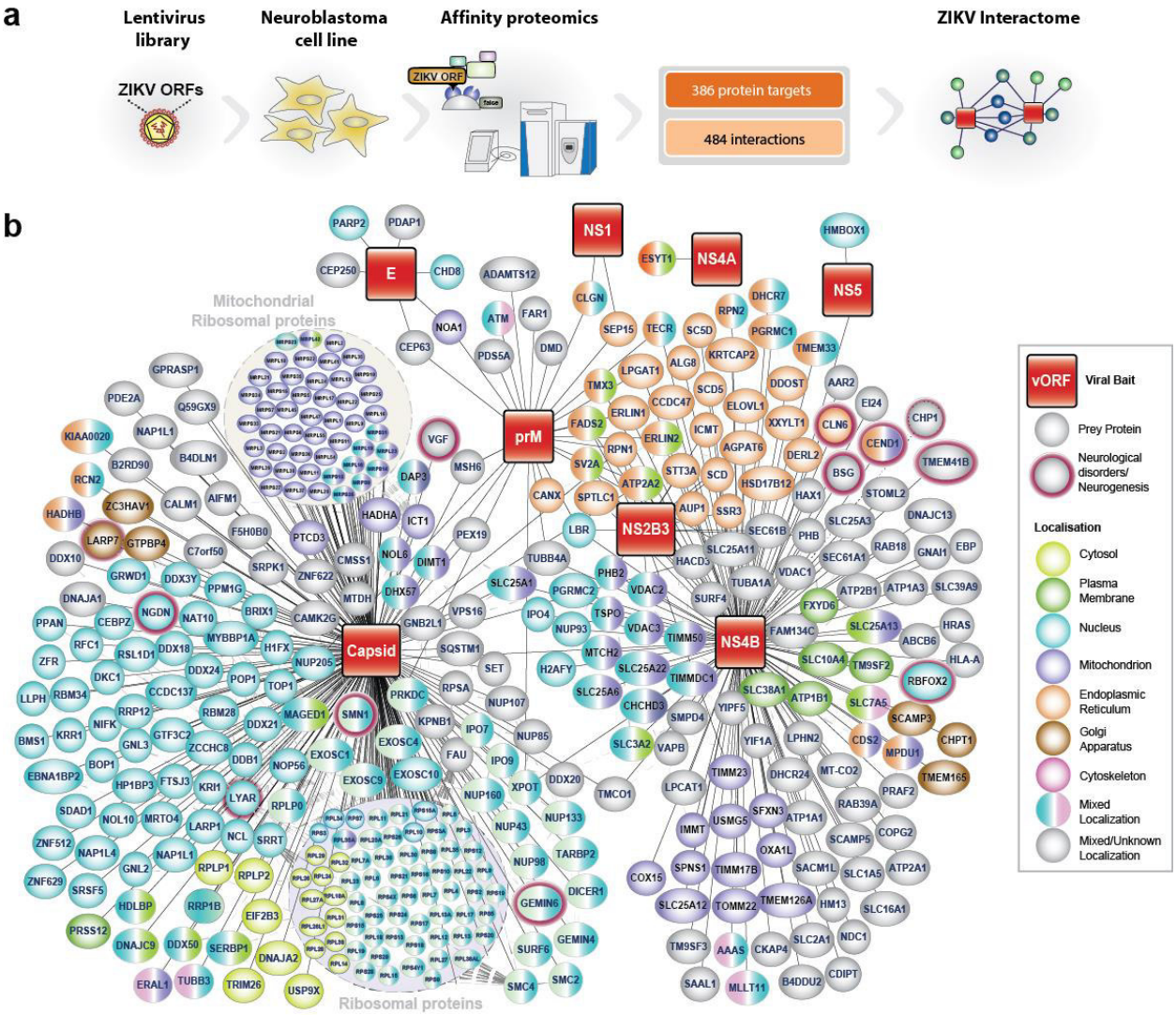

Figure 1 – A ZIKV-host protein-protein interaction network in neuronal cells

(a) Affinity-purification of ZIKV proteins and interactome generation strategy. (b) Network representation of the high-confident ZIKV-host interactome in SK-N-BE2 cells. There are 8 ZIKV bait proteins (red squared nodes) and 386 interacting host proteins (ellipse nodes) (All baits: Log_2(Fold-change) ≥ 2.5; p-value ≤ 0.05; Capsid: Log_2(Fold-change) ≥ 2.5; p-value ≤ 5×10^{-5}). Interactions of ZIKV and host proteins are indicated by black lines. Published physical associations of the host proteins are indicated by dotted

grey lines. Subcellular localization (color of nodes) of host protein is taken from Gene Ontology. Proteins with known functions in neurogenesis or neurological diseases are circled in pink.

Figure 2

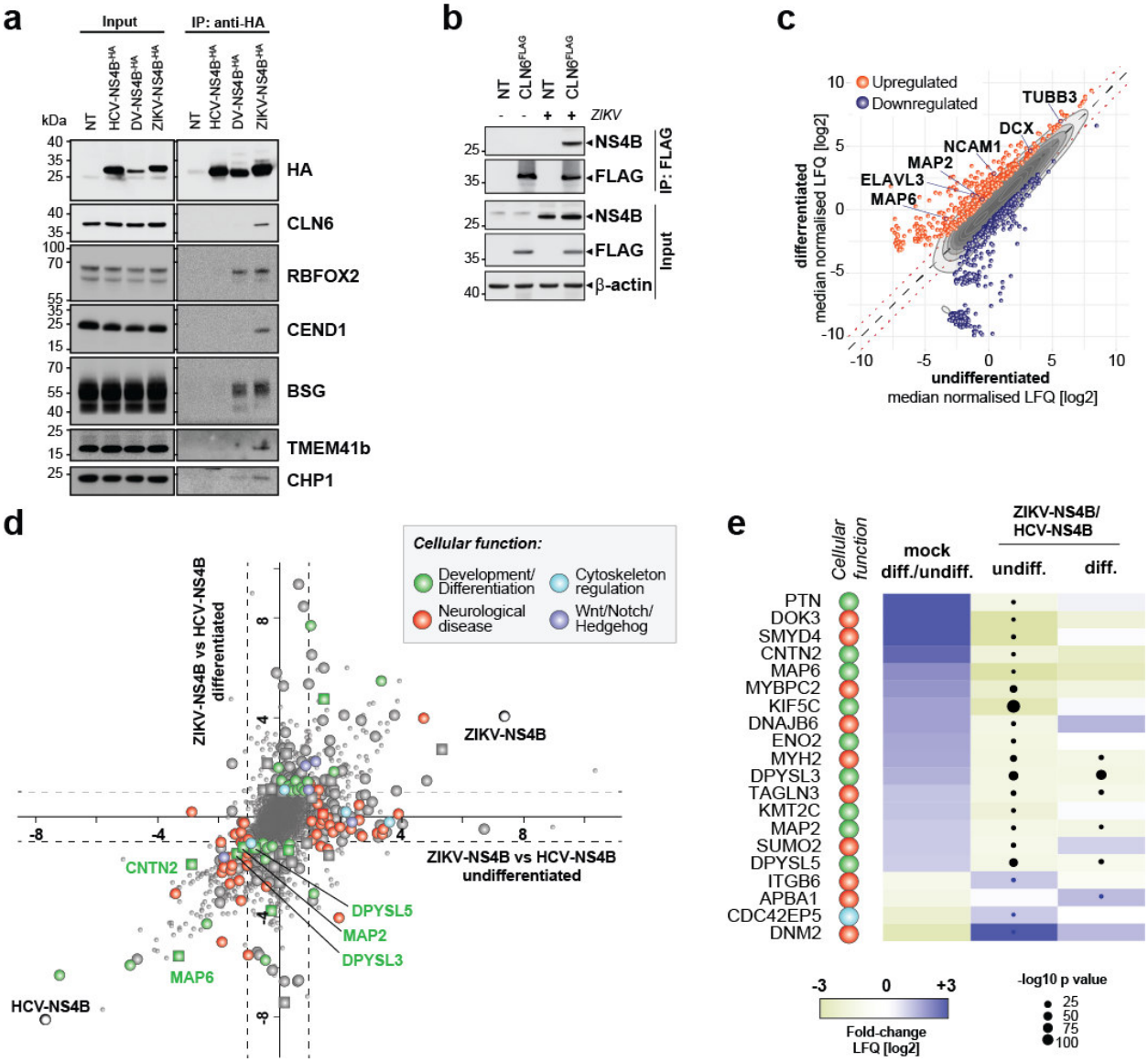

Figure 2 – Validation of NS4B interacting proteins and impact of ZIKV and NS4B on hNPC proteome upon differentiation

(**a**) Co-immunoprecipitation of ZIKV-NS4B-HA with endogenous host proteins. Cell lysates of SK-N-BE2 cells transduced with empty lentiviruses (NT) or lentivirus-expressing HA-tagged HCV-, DENV- or ZIKV-NS4B proteins were used for HA-immunoaffinity purification and probed with the indicated antibodies. Representative experiment of three is shown. (**b**) Reciprocal co-immunoprecipitation of NS4B with FLAG-tagged CLN6. SK-N-BE2 cells transiently transduced with empty lentiviruses (NT) or lentivirus-expressing FLAG-tagged CLN6 were infected with ZIKV (H/PF/2013) and FLAG-immunoprecipitated proteins probed

with NS4B-specific antibodies. Representative experiment of three is shown. (**c**) Comparative proteomic analysis of differentiated hNPC that were left untreated (undifferentiated) or differentiated for 5 days in the presence of ROCK inhibitor. Their global proteome was analyzed by quantitative LC-MS/MS. Significantly up- or down-regulated proteins (p-value ≤ 0.01; $|Log_2(\text{Fold-change})| \geq 1$) are shown in orange and blue, respectively; highlighted proteins are known markers of neuronal differentiation. (**d**) Impact of ZIKV-NS4B on differentiated and undifferentiated hNPC. hNPC were transduced with ZIKV- or HCV-NS4B and cultured as described above. The scatter plot displays ZIKV-NS4B specific changes (compared to HCV-NS4B). Proteins non-significantly changing are shown as small grey circles; proteins specifically modulated by ZIKV-NS4B are shown as large circles or squares. Color codes refer to functional annotations; squares indicate proteins significantly modulated by ZIKV-NS4B which are specifically up- or down-regulated during differentiation as in (c). (**e**) Protein levels of cellular factors differentially modulated upon hNPC differentiation and ZIKV-NS4B-transduction. Ratios of protein abundance in naïve hNPC (differentiated/undifferentiated), differentiated hNPC (ZIKV-NS4B/HCV-NS4B) or undifferentiated hNPC (ZIKV-NS4B/HCV-NS4B). Colored squares indicate functional annotations as in (d), while up- or down-regulated proteins are displayed in shades of blue or green, respectively. All significant changes are indicated by black circles; sizes correspond to indicated p-values.

Figure 3

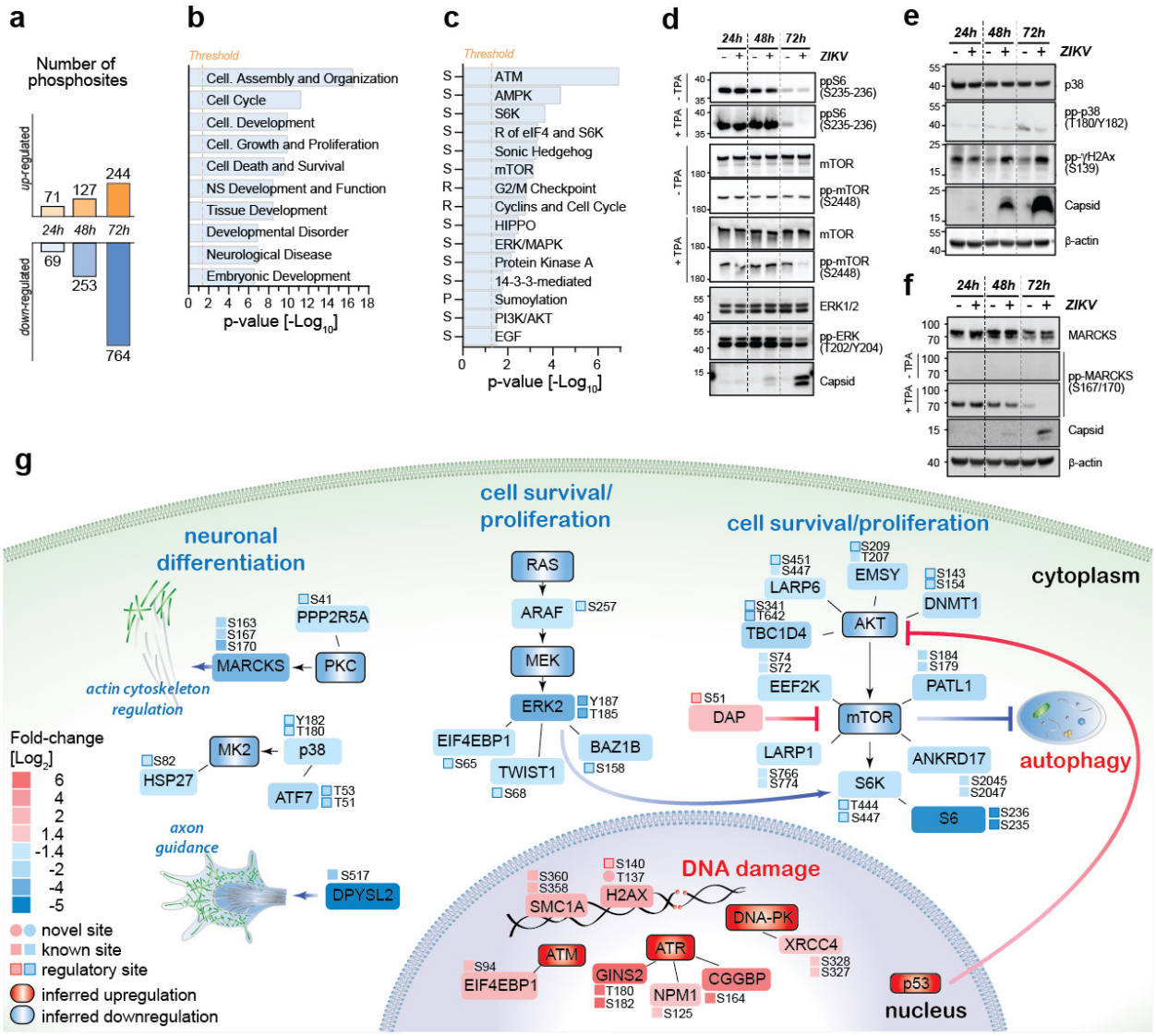

Figure 3 – Global phosphoproteomic profiling of ZIKV-infected cells

SK-N-BE2 cells were either mock-infected or infected with ZIKV (MOI=3) and ZIKV-specific phosphoproteomic changes at different time points were analyzed by LC-MS/MS. (**a**) Total number of up- or down-regulated class I phosphosites significantly regulated by ZIKV infection 24, 48 and 72 hours post-infection (p-value ≤ 0.01; $|Log_2$ (Fold-change)| ≥ 1). (**b**) Biological functions and (**c**) canonical pathways modulated by ZIKV infection (IPA, Fisher's exact test p-value <0.05) (S – signaling; R – regulation; P – pathway); (**d**, **e**) Cellular lysates of SK-N-BE2 cells mock-infected or infected with ZIKV at different time points were probed with phospho- or virus-specific antibodies as specified on the right. Where indicated,

samples were treated with TPA (32 nM) 15´ before lysis. (**g**) Selected cellular pathways perturbed by ZIKV showing significantly up- or down-regulated phosphosites. Colors of protein nodes indicate measured (Log_2 (fold-change) of strongest phosphosite change) or inferred regulation of the proteins central to canonical pathways and/or their substrates. Individual phosphosites are shown next to the corresponding molecules (colors indicate the highest Log_2(fold-change) over time). Newly identified phosphosites are presented as circles, known phosphosites are shown as squares, while regulatory sites are marked with framed squares. Arrows signify positive regulation of downstream proteins, while blunt-ended lines – negative regulation.

Figure 4

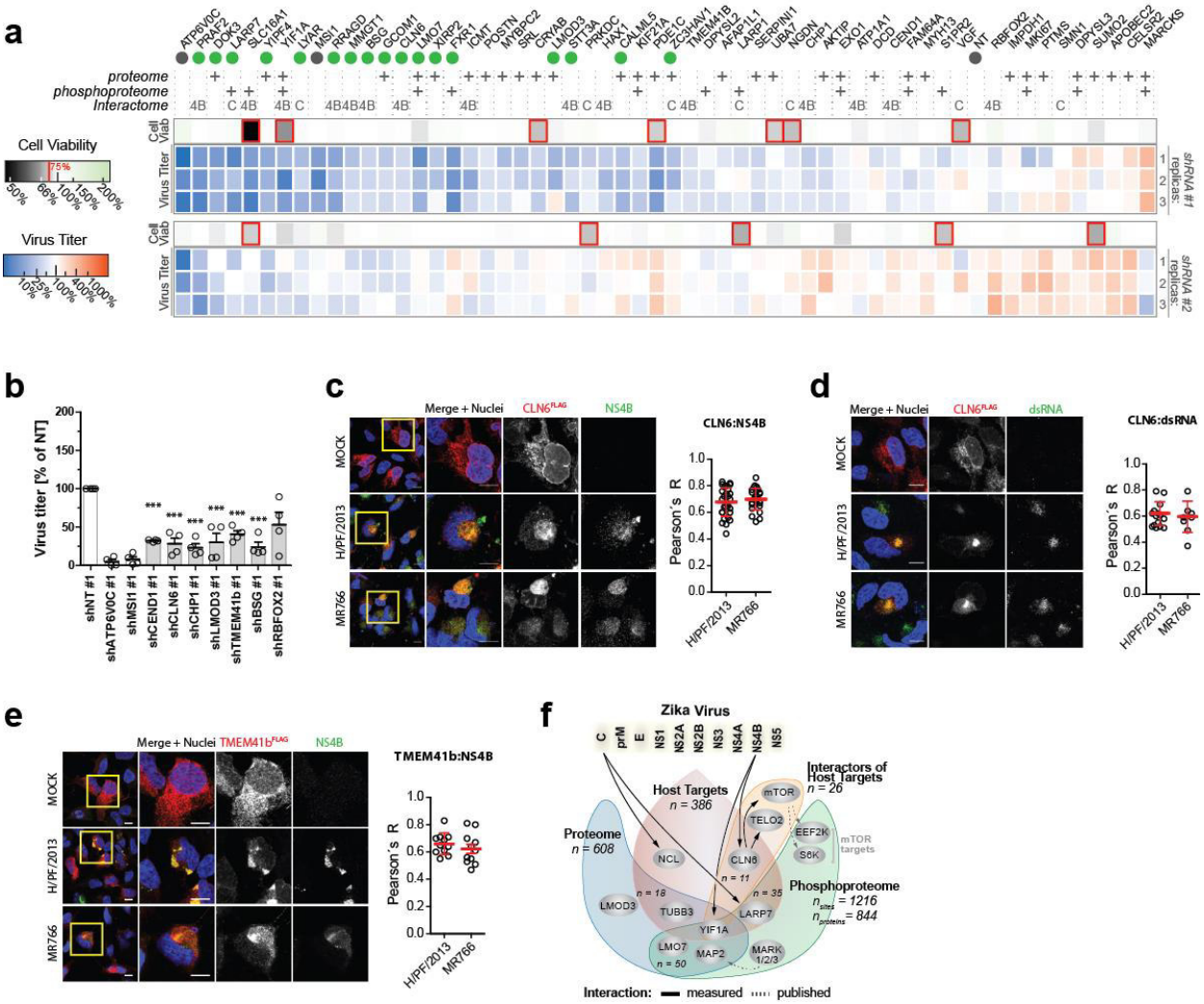

Figure 4 – shRNA screen identifies novel ZIKV host-dependency factors

(**a**) SK-N-BE2 cells were transduced with individual shRNAs targeting genes modulated by ZIKV at the proteomic or phosphoproteomics level, or specifically bound by ZIKV viral proteins, and ZIKV replication measured by PFU assay. Results are presented as heat map and were normalized according to cells treated with non-targeting (NT) shRNA. NT controls and shRNAs targeting ATP6V0C and MSI1 are highlighted with grey circles, and served as internal controls for lentiviral transduction and inhibition of virus replication, respectively. shRNAs exerting cytotoxic effects are indicated by red squares (normalized median cell viability < 75% of NT-controls). Results from three independent experiments for each shRNA are shown in each row. The genes are ordered by the average rank of median fold-change. The following criteria were applied to select hits (highlighted with green circles): ≥50% decrease in viral replication with

both shRNAs each, or ≥75% with any shRNA. (**b**) Validation of silencing efficiency and gene knock-down effects on ZIKV replication on selected host factors from (a). Data are mean and s.d. of quadruplicate infections. Asterisks indicate significance to NT control (student t-test; p-value≤0.001). (**c**, **d**, **e**) hNPC cells were transduced with CLN6 or TMEM41b-expressing lentiviruses (MOI=3) and mock-infected (mock) or infected with ZIKV H/PF/2013 or MR766 (MOI=5). Fixed cells were immunostained 24h later for dsRNA, ZIKV-NS4B and FLAG-tagged proteins as indicated. Boxed areas are enlarged in upper-right panels. Scale bar represents 10 µm. Graphs on the right-hand side of each panel display the mean and standard deviation of Pearson's correlation coefficients, each dots represent 1 cell. (**f**) Intersection of ZIKV interactome, proteome and phosphoproteome data sets highlighting characteristic proteins perturbed at multiple levels. ZIKV proteins (yellow boxes) interact with host proteins (beige area), potentially affecting their normal interactions (orange). ZIKV infection perturbs phosphorylation (green) of its host targets (e.g. LARP7) and along signaling pathways (EEF2K and S6K via CLN6-mTOR-TELO2; or MAP2 via MARK1/2/3). Protein levels (blue) are also affected and carry, among the others, signatures of ZIKV-induced changes to vesicle transport (YIF1A) and neuronal differentiation pathways (MAP2). Protein interactions measured in this study are shown by solid arrows; grey dotted arrows represent published interactions. The numbers correspond to proteins significantly changed in a given data set or data sets intersection.

Extended Data Figure Legends

Extended Data Figure 1

a

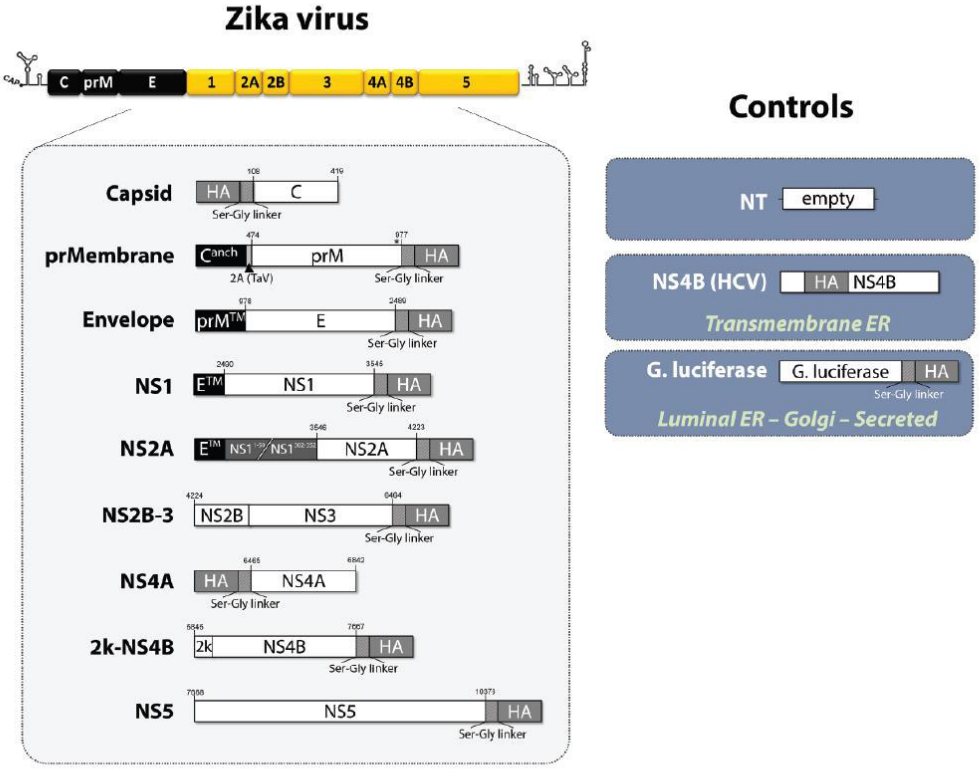

b

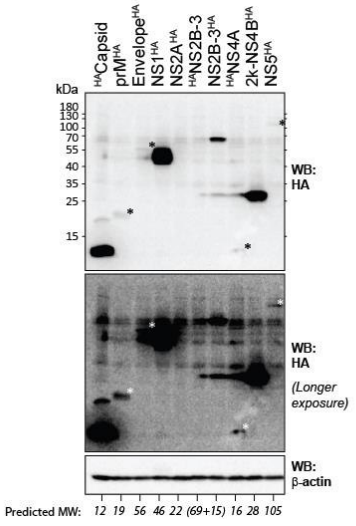

c

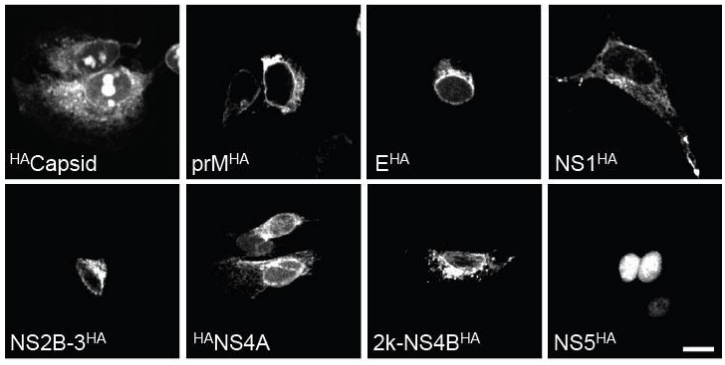

Extended Data Figure 1 - Design rationale, expression and sub-cellular localization of HA-tagged ZIKV proteins.

(**a**) Schematic representation of ZIKV HA-tagged viral proteins and controls used in this study. The full-length ZIKV genome is shown at the top, with the 5' and 3' NTRs depicted with their putative secondary structures. Polyprotein cleavage products are separated by vertical lines and labeled as specified. The individual open reading frames (ORFs) of each ZIKV proteins were fused with an HA epitope either at their N- or C-termini as depicted. Numbers above each sequence refer to the nucleotide sequence of the ZIKV isolate FSS13025 used as reference (GeneBank: KU955593.1). To ensure the correct sub-cellular localization and protein topology, the sequence of the Capsid anchor (C^{anch}), the transmbembrane domain of prM (prM^{TM}) and the transmembrane domain of Envelope (E^{TM}) were fused at the N-termini of prMembrane, Envelope and NS1, respectively. Additionally, given the complex topology of NS2A, the E^{TM}, and a fusion protein encoding the first and the last 50 aminoacids of NS1 was fused at its N-terminus. As additional controls, an empty pWPI-lentiviral vector (NT), or HA-tagged non-structural protein 4B of Hepatitis C virus (NS4B-HCV) and Gaussia luciferase (G. luciferase) were included to monitor for non-specific binding to the anti-HA beads as well as organelle-dependent enrichment artifacts in AP-MS/MS analysis. (**b**) Intracellular levels of ZIKV proteins in lentivirus-transduced SK-N-BE2 cells. SK-N-BE2 cells were transduced with lentiviruses encoding for each ZIKV protein at an MOI of 3, and seventy-two hours later cell lysates clarified by centrifugation were used for western-blotting against HA and β-actin. Numbers on the left refer to molecular weight standards given in kDa. Asterisks mark protein expressed to a lower level, which can be observed upon longer exposure of the membrane. Note that c-terminally tagged NS2A and n-terminally tagged NS2B-3 could not be detected, while c-terminally tagged NS2B-3 fusion protein was expressed at the expected molecular weight, and was therefore used for further experiments in this study. The bottom lane indicates the predicted molecular weight of each viral protein in kDa. (**c**) Subcellular localization of ZIKV proteins in lentivirus-transduced SK-N-BE2 cells. SK-N-BE2 cells were seeded in 24-well plates and transduced as described above. Seventy-two hours post-transduction viral proteins were detected using rabbit anti-HA antibody and Alexa-fluor488 conjugated secondary antibody and imaged by confocal microscopy. Scale bar, 10 μm.

Extended Data Figure 2

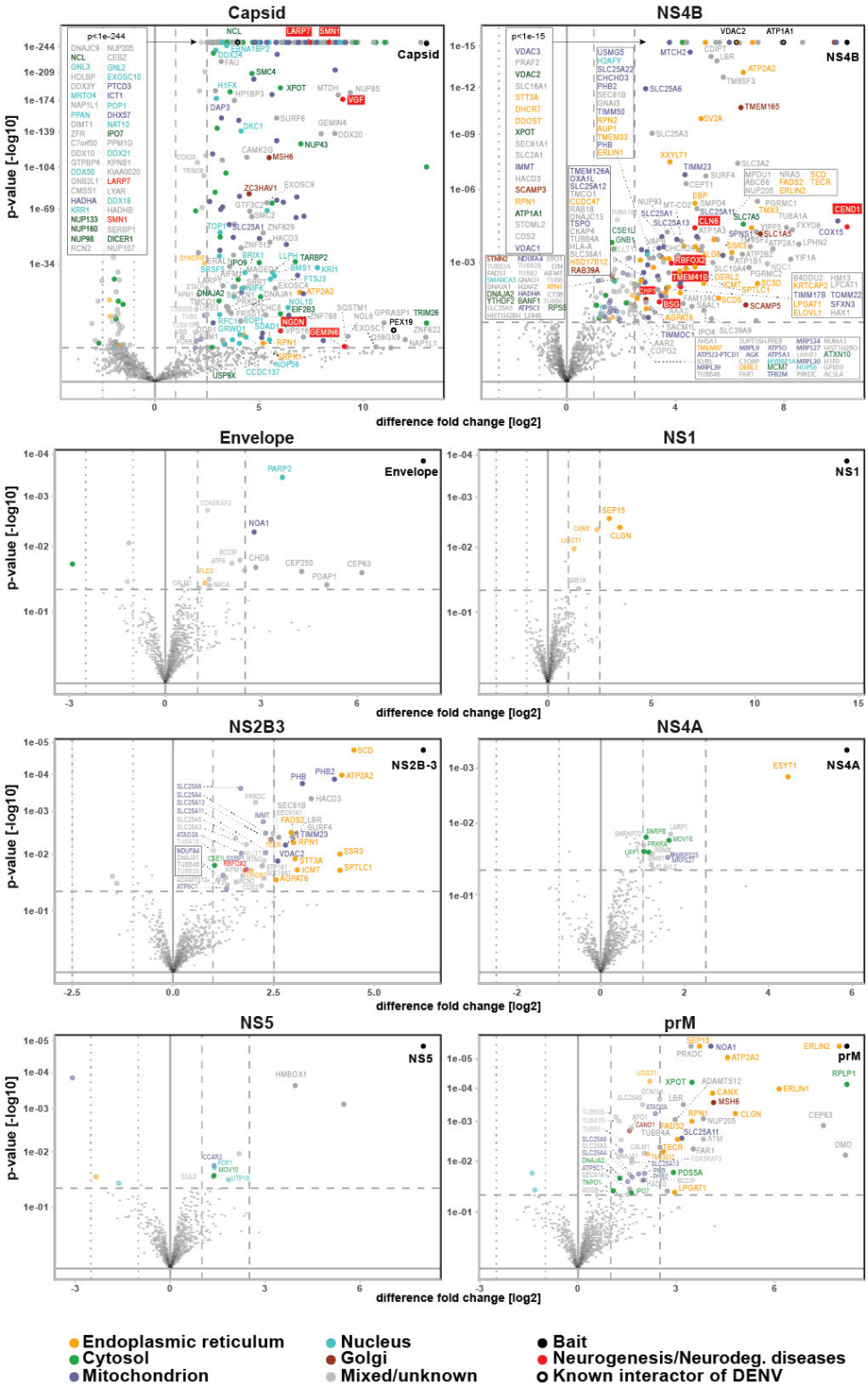

Extended Data Figure 2 - Volcano plots of individual ZIKV-interacting proteins.

Volcano plots of label-free Affinity-Purification (AP) LC-MS/MS of individual ZIKV proteins. Each volcano plot displays all identified proteins (median $\log_2$ fold-change of bait-specific protein enrichment in comparison to the background plotted against the corresponding $-\log_{10}$ *P*-value). Dotted grey lines represent the $\log_2$ fold-change and P value cut-offs used. High-confident interactors ($\log_2$ (Fold-change) ≥ 2.5, *p*-value ≤ 0.01) are labelled according to their sub-cellular localization. In case of Capsid, due to its highly hydrophobic character and multiple subcellular localizations, more stringent *P*-value cut-off was used (*p*-value ≤ $5x10^{-5}$) and ribosomal proteins were not individually labelled. The respective viral bait of each AP is shown in black, black circles represent known DENV target proteins while proteins with roles in neurogenesis, neurodegenerative diseases or infertility are labelled in red.

Extended Data Figure 3

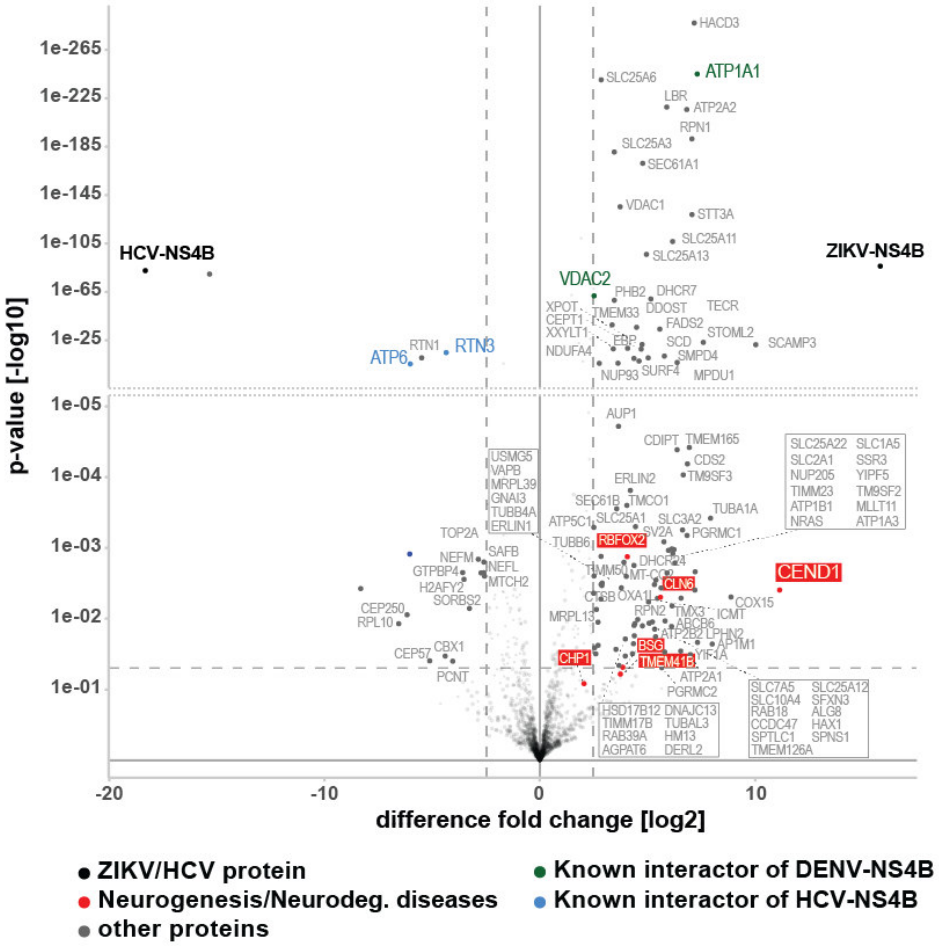

Extended Data Figure 3 - Volcano plots of ZIKV-NS4B and HCV-NS4B-interacting proteins.

Volcano plot comparing the specificity of protein enrichment in ZIKV-NS4B versus HCV-NS4B AP (median $\log_2$ fold-change plotted against $-\log_{10}$ *p*-value for ZIKV-NS4B versus HCV-NS4B). Specific NS4B-interacting proteins are labelled as described in Extended Data Figure 2. Previously reported interactors of HCV-NS4B, or the ZIKV closely-related DENV-NS4B are shown in blue and green, respectively.

Extended Data Figure 4

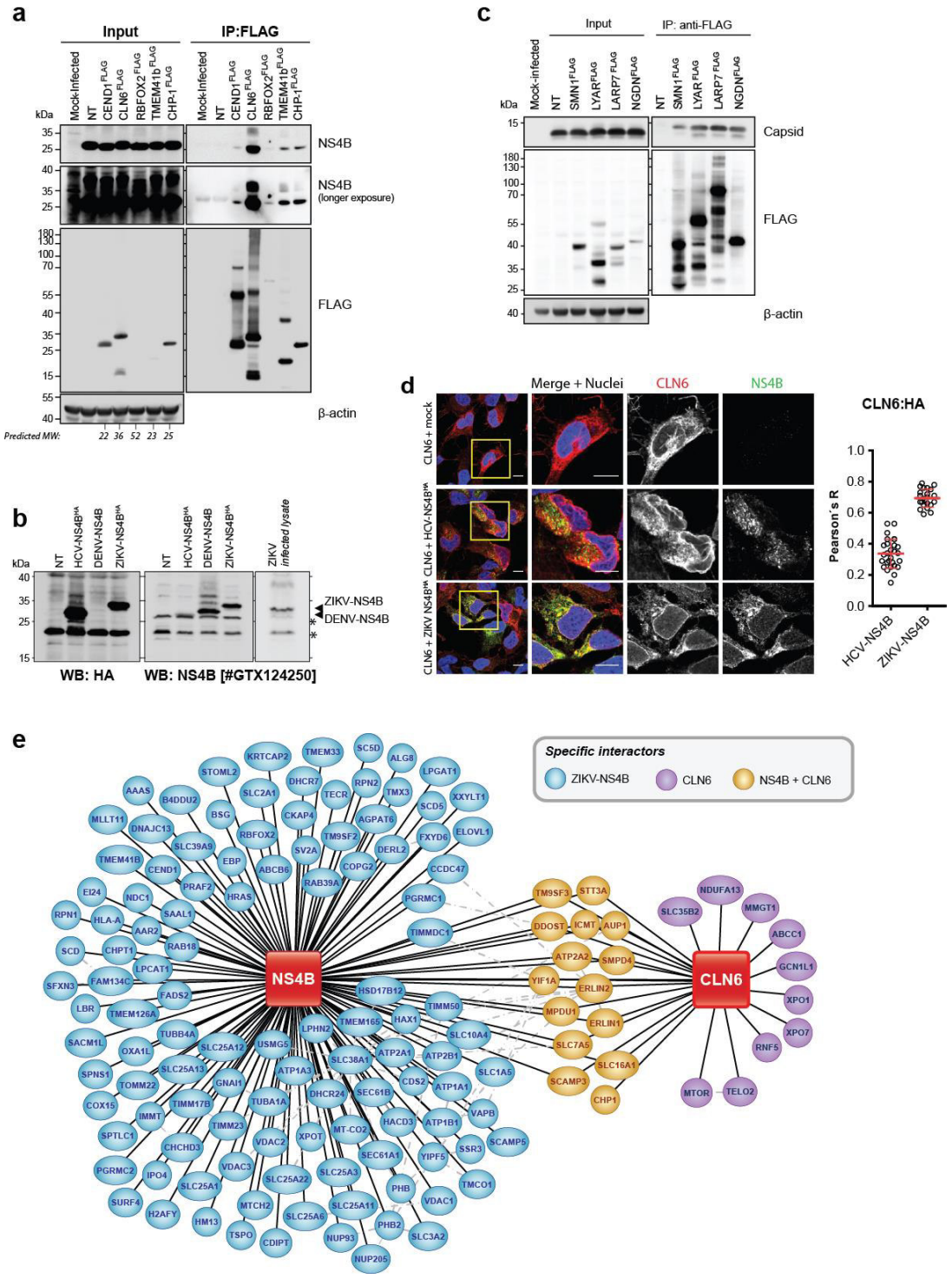

Extended Data Figure 4 - Validation of NS4B interacting proteins upon ZIKV infection.

(a) Reciprocal co-immunoprecipitation of NS4B with FLAG-tagged host factors. SK-N-BE2 cells transiently transduced with empty lentiviruses (NT) or lentiviruses expressing FLAG-tagged CEND1,

CLN6, TMEM41b, RBFOX2 and CHP1 were mock-infected or infected with ZIKV H/PF/2013 (MOI=1) and three days later FLAG-immunoprecipitated proteins probed with ZIKV NS4B-specific antibody. The bottom lane indicates the predicted molecular weights of each viral protein in kDa. Representative experiment of three is shown. (b) Validation of anti-DENV-NS4B-specific antibody for immunodetection of ZIKV-NS4B. SK-N-BE2 cells were transiently transduced with empty lentiviruses (NT) or lentiviruses expressing HCV-NS4B-HA, DENV-NS4B or ZIKV-NS4B-HA, and 72 hours later probed consecutively with mouse anti-HA (left panel) or rabbit anti-DENV-NS4B specific antibodies. ZIKV-infected SK-N-BE2 cell lysates, shown on the right-end side, were included as control. Asterisks indicate unspecific bands. (c) Reciprocal co-immunoprecipitation of Capsid with FLAG-tagged host factors. SK-N-BE2 cells transiently transduced with empty lentiviruses (NT) or lentiviruses expressing FLAG-tagged SMN1, LYAR, LARP7 and NGDN were infected as described above and FLAG-immunoprecipitated proteins probed with ZIKV Capsid-specific antibody. Representative experiment of two is shown. (d) hNPC were transduced with lentiviruses expressing Flag-tagged CLN6 alone (mock) or co-transduced with lentiviruses expressing HCV-NS4B-HA or ZIKV-NS4B-HA (3 MOI), stained with FLAG- and HA-specific antibodies and imaged by confocal microscopy. Boxed areas are enlarged on the right. Graphs on the right-hand side of each panel display the mean and standard deviation of Pearson's correlation coefficients (each dot represent 1 cell). Scale bar represents 10 µm. The panel on the right hand (e) Network representation of CLN6-interacting cellular proteins and comparison with the ZIKV-NS4B interactors. AP-MS/MS analysis of FLAG-tagged CLN6 in SK-N-BE2 cells revealed novel CLN6-specific interacting proteins (displayed in magenta; i.e. TELO2 and mTOR) as well as shared cellular interactors with ZIKV-NS4B (displayed in yellow, i.e. ICMT, STT3A). Solid lines represent specific interactors identified by AP-MS/MS analysis, grey dotted lines represent previously published protein-protein interactions.

Extended Data Figure 5

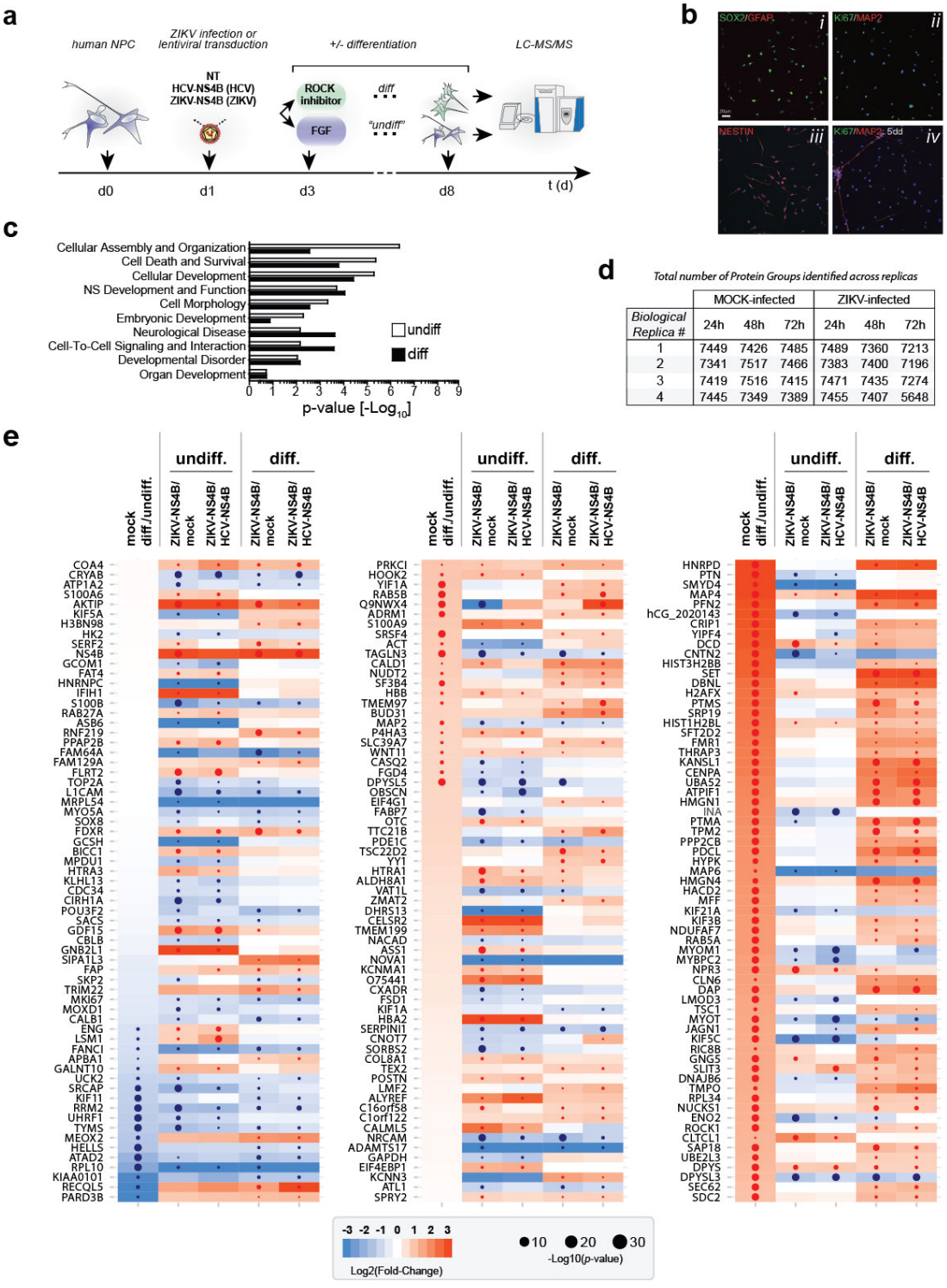

	MOCK-infected			ZIKV-infected		
Biological Replica #	24h	48h	72h	24h	48h	72h
1	7449	7426	7485	7489	7360	7213
2	7341	7517	7466	7383	7400	7196
3	7419	7516	7415	7471	7435	7274
4	7445	7349	7389	7455	7407	5648

Extended Data Figure 5 – Effects of ZIKV infection or NS4B transduction on undifferentiated or differentiated hNPC

(a) Experimental approach used for hNPC differentiation. hNPC cells were transduced with empty (NT), HCV-NS4B-HA or ZIKV-NS4B-HA-expressing lentiviruses (MOI=3), mock-infected or infected with ZIKV (H/PF/2013) (MOI=0.01). Forty-eight hours later, differentiation was induced for 5 days by growth factor withdrawal and addition of 10 µM ROCK inhibitor, while undifferentiated cells were kept in NPC media in the presence of bFGF. Cell pellets were next used for quantitative label-free LC-MS/MS-based profiling of the global proteome. (b) Characterization of hNPC cells used for proteomic analysis. Undifferentiated hNPC kept in the presence of bFGF were stained with (i) SOX2 and GFAP, (ii) Ki67 and MAP2 and (iii) Nestin-specific antibodies. Alternatively, hNPC cells differentiated 5 days in the presence of a ROCK inhibitor were stained with Ki67 and MAP2-specific antibodies (iv). Under proliferating conditions hNPC expressed KI67, SOX2 and NESTIN, confirming maintenance of their proliferative state in the presence of FGF. No neuron-specific protein MAP2 or astrocyte marker GFAP were detected under these conditions. After differentiation for 5 days in vitro in the presence of ROCK inhibitor, neuronal marker MAP2 was upregulated while proliferation marker KI67 was downregulated, suggesting commitment towards the neuronal lineage. (c) Cellular processes enriched in NS4B-ZIKV changes in proliferating or differentiating hNPC. (d) Total number of proteins identified across biological replicates (n=4) and conditions. (e) Heat Map of all significant (p-value ≤ 0.01, $|\text{Log}_2\text{ (Fold-change)}| \geq 1.0$) changes occurring upon proliferation and differentiation conditions in NS4B-ZIKV transduced cells in comparison to NS4B-HCV and mock transduction.

Extended Data Figure 6

a

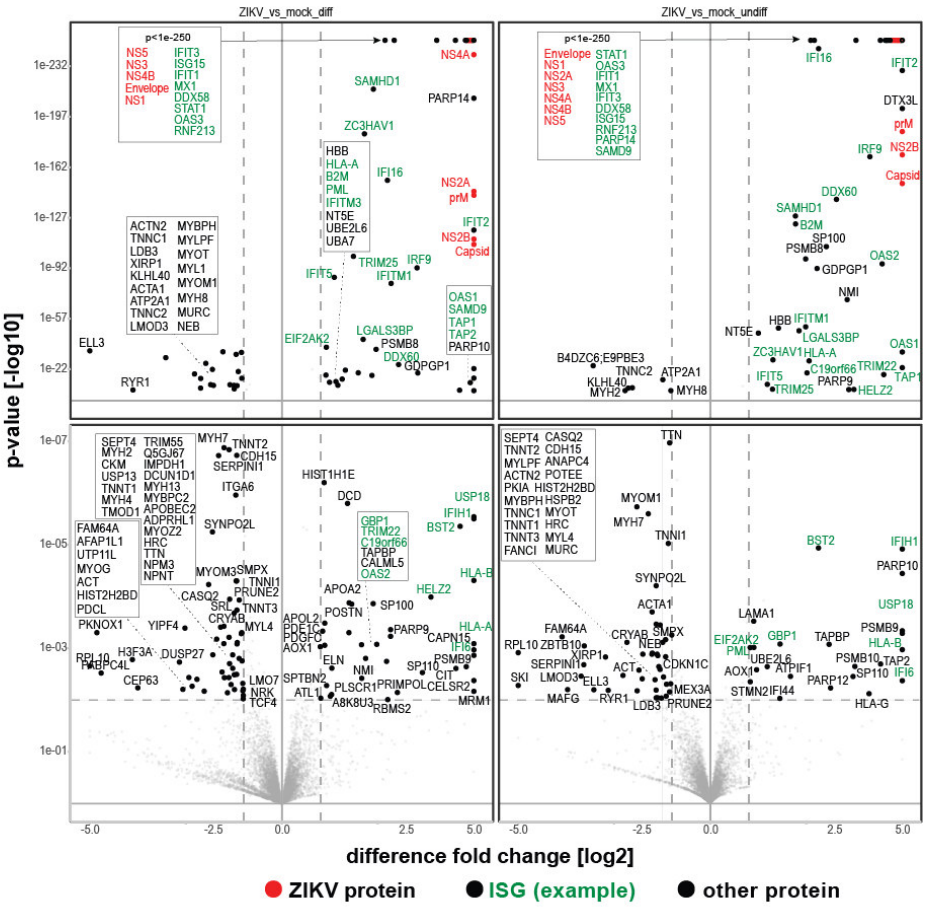

b

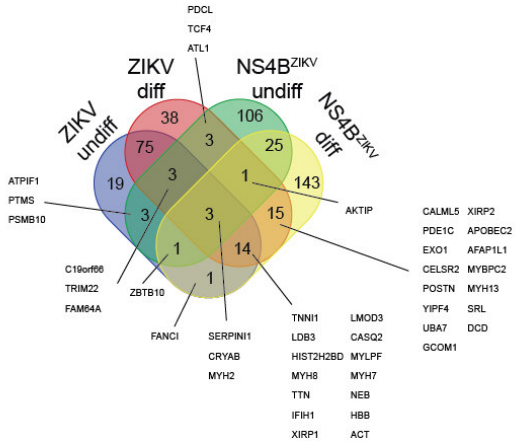

Extended Data Figure 6 – Global proteomic analysis of ZIKV-specific effects in differentiating or proliferating hNPC

(a) hNPC cells were mock-infected or infected with ZIKV (H/PF/2013, MOI=0.01) and cultured under proliferating or differentiating conditions as described in Fig. S5a. Volcano plots display proteins significantly up- or down-regulated by ZIKV-infection in differentiated (left panel) or undifferentiated (right panel) hNPC. Viral proteins are labeled in red. Proteins with functions in antiviral immunity are labeled in green. Significance cutoffs are indicated by the dashed grey lines ($|\text{Log}_2(\text{Fold-change})| \geq 1$; p-value ≤ 0.01). (b) Venn diagram displaying the total number of significantly up- or down-regulated proteins in every experimental condition ($|\log_2(\text{Fold-change})| \geq 1$; *p*-value < 0.01) and the total number and gene names of significantly modulated proteins similarly regulated by ZIKV infection or ZIKV-NS4B transduction upon differentiation (diff) or proliferation (undiff).

Extended Data Figure 7

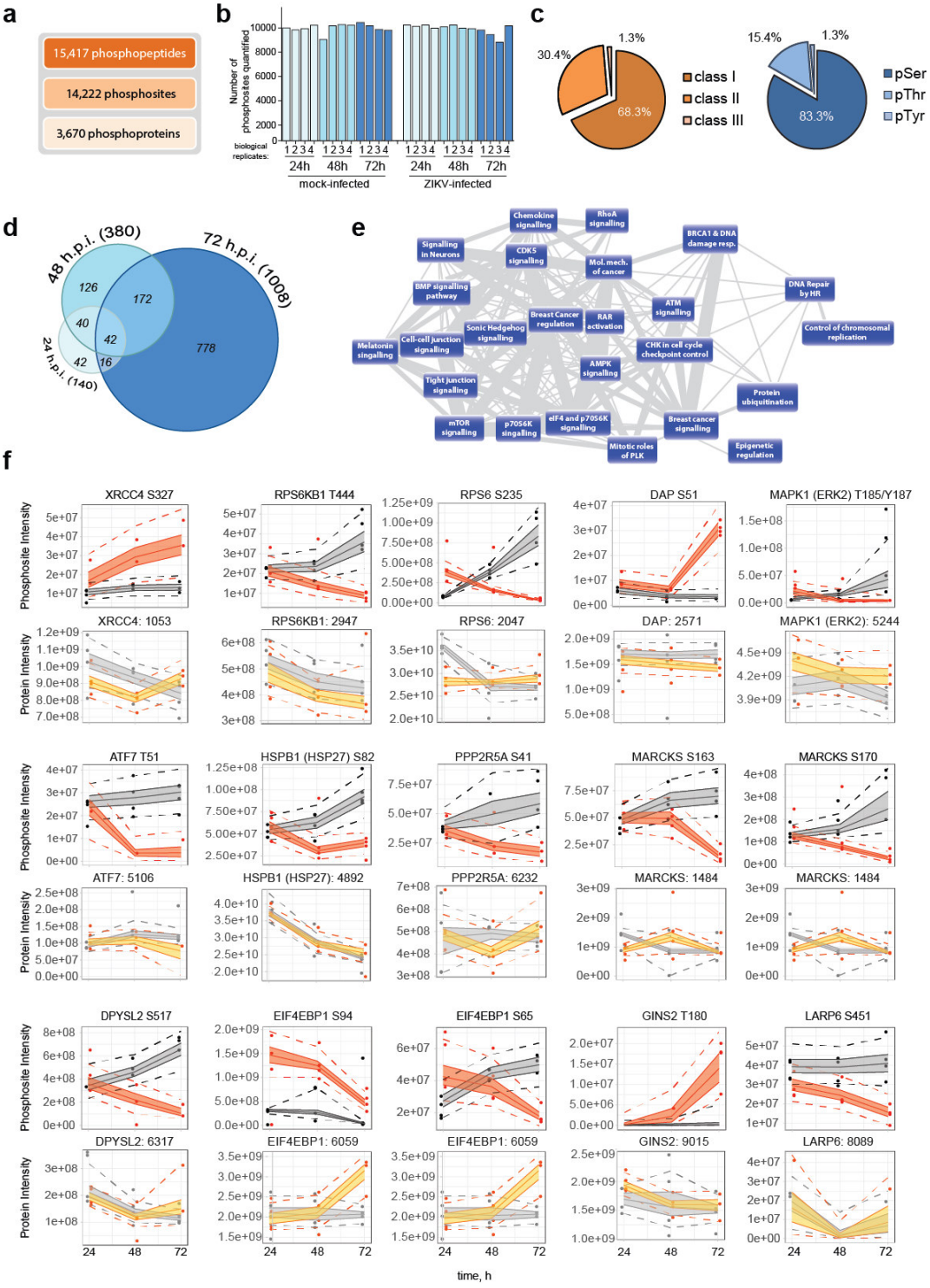

Extended Data Figure 7 – Time-resolved phosphoproteomic analysis of ZIKV-infected SK-N-BE2 cells

(a) Total number of phosphopeptides, phosphosites and phosphoproteins identified in this study. (b) Total number of phosphosites identified across biological replicates and conditions (n=4). (c) Relative percentage of Class I, II and III phosphosites (localization probability>0.75) and phosphorylation of specific pSer, pThr, pTyr. (d) Venn diagram of significantly changing phosphosites at 24, 48, 72 hours post infection. (e) Network analysis of cellular processes significantly modulated by ZIKV infection at phosphorylation level (IPA). Nodes are canonical pathways identified with Fisher's exact test (*p*-value ≤ 0.05); edges are shared proteins between the pathways. (f) Profile plots of significantly changing phosphosites, mapped to pathways in Fig. 3d, and their corresponding total protein levels at 24, 48 and 72 hours after ZIKV infection (orange for phospho levels, yellow for protein levels) or mock treatment (grey). Numbers next to protein names refer to unique MaxQuant Protein Groups ID (Supplementary Table 5). Points are normalized intensities of individual replicates, solid line is median, filled area corresponds to 25-75 percentiles, dashed lines mark 2.5-97.5 percentiles of the posterior distribution.

Extended Data Figure 8

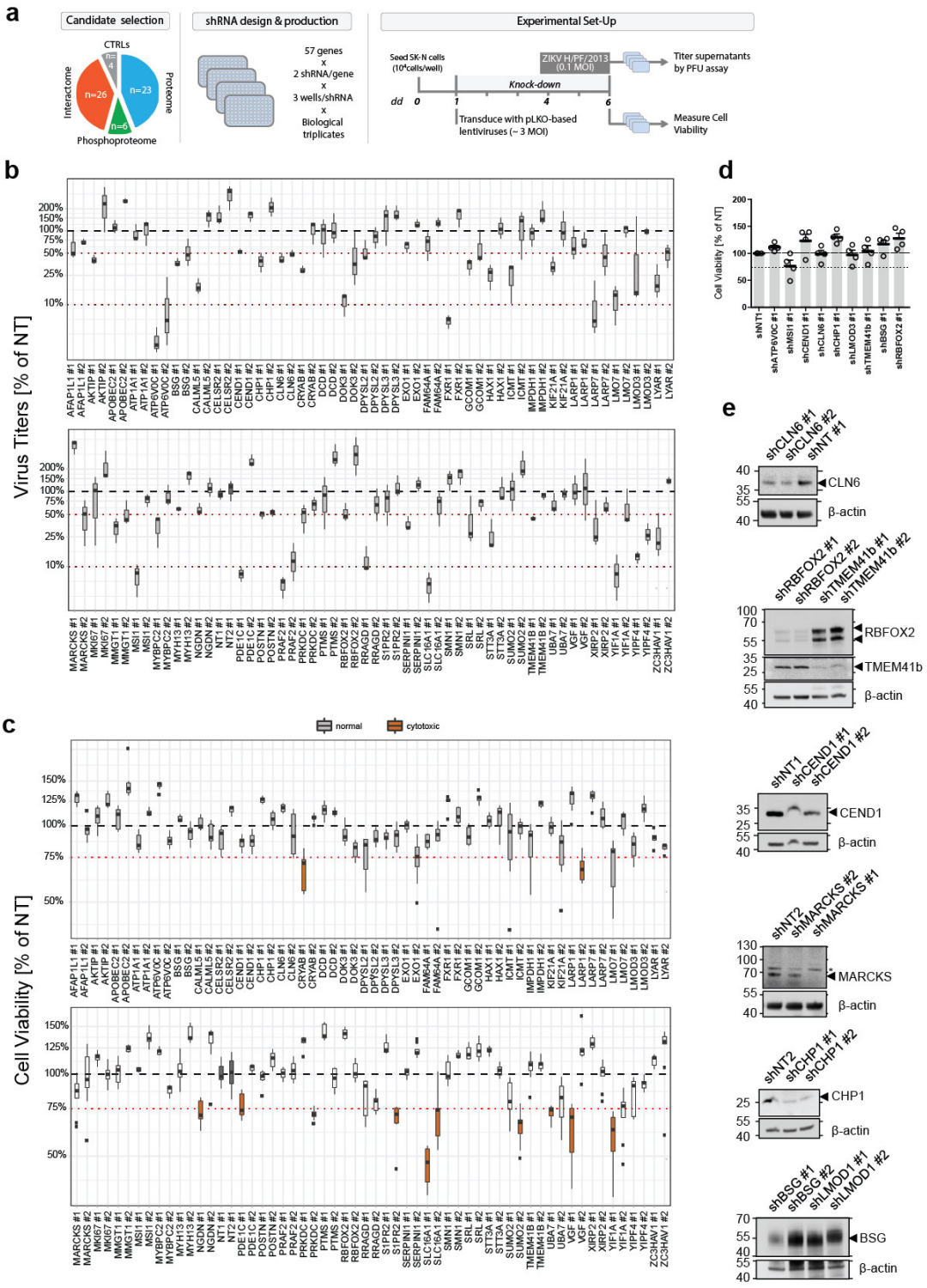

Extended Data Figure 8 – Effect of shRNA-mediated silencing of ZIKV-modulated host proteins on viral replication

(a) Schematic representation of the experimental set-up used for the shRNA screen. Target genes were selected among the cellular host factors specifically binding ZIKV-Capsid or -NS4B (Interactome; n=26), significantly regulated at the phosphoproteomic level by ZIKV infection (n=6) or significantly regulated at the proteomic level both by ZIKV infection and ZIKV-NS4B-expression in hNPC (n=23). Controls included non-targeting shRNA of two different pLKO-based lentivirus generations (NT1 and NT2) used as reference; and shRNAs targeting the ATP6V0C and Musashi1, which impairs flavivirus pH-dependent viral entry and ZIKV replication, respectively [40,41]. Two individual shRNAs/gene were selected from the MISSION TRC library (Sigma-Aldrich), and used for lentivirus production in 293Ts as described in *Methods*. SK-N-BE2 cells were transduced with individual lentiviruses (3 wells/shRNA) in three independent experiments. Three days post-transduction cells were infected with ZIKV H/PF/2013 (MOI=0.1) and 48 hours later virus-containing supernatants used for titration by PFU assay. The cellular viability was assessed with a Resazurin-based assay performed in parallel. (b-c) ZIKV titers and cell viability upon knock-down of selected host-factors. Viral titers, as determined by PFU assay, and cell viability, as determined by Resazurin assay, are expressed as % of non-targeting controls (n=3). (d) Cell viability of SK-N-BE2 cells upon knock-down of selected host factors (n=4, related to Fig. 4b). (e) Validation of the silencing efficiency of selected shRNA targeting ZIKV host-factors. The gene silencing was evaluated for each cellular protein via Western blot detection using the antibodies specified on the right. Asterisks indicate non-specific signal, numbers on the left indicate molecular weight markers expressed in kDa.

Extended Data Figure 9

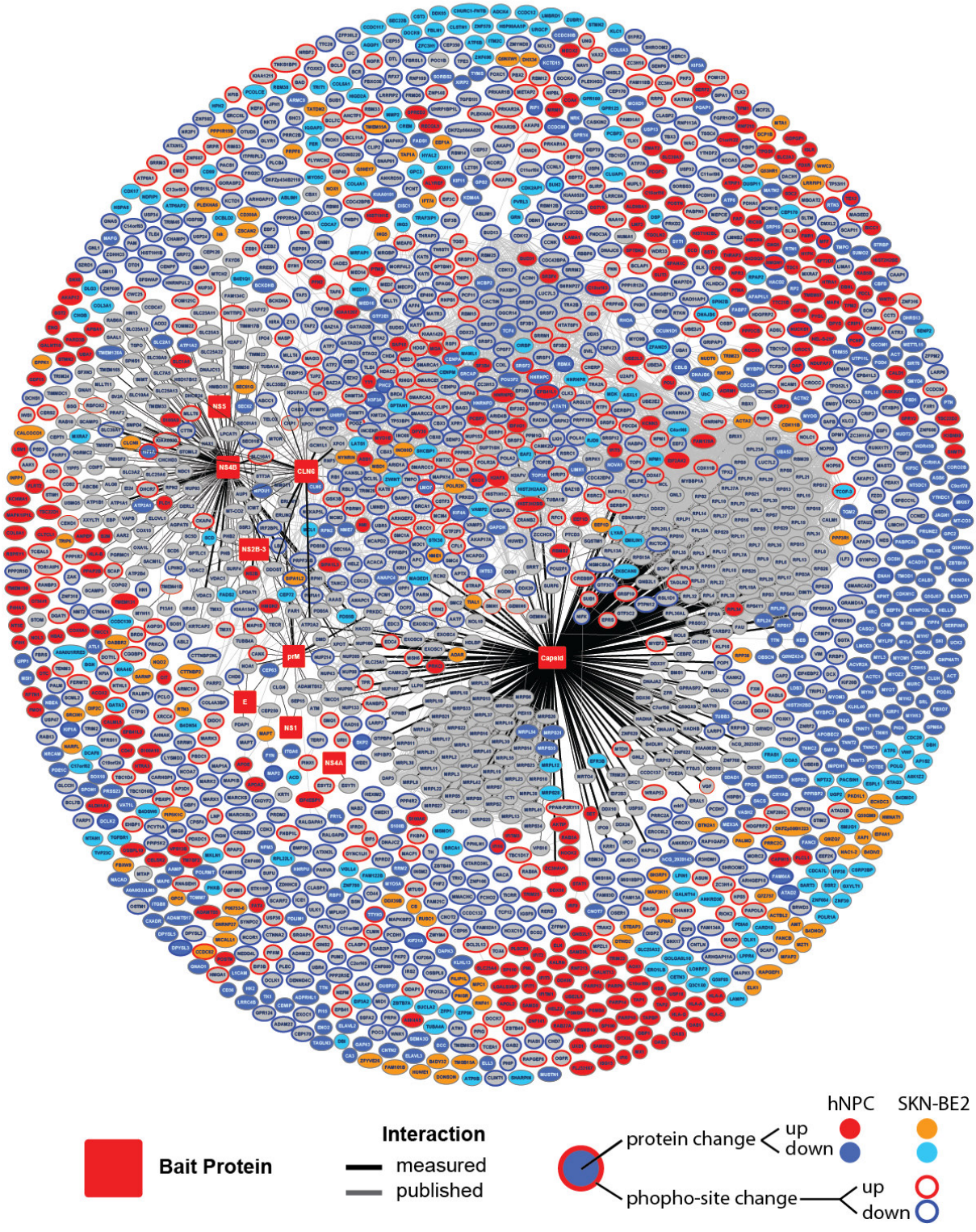

Extended Data Figure 9 – Integration of data from orthogonal proteomic screens and protein-protein interaction databases

Integrated network of ZIKV protein interactors, CLN6-interacting cellular proteins, proteins changing at proteome and/or phosphoproteome levels plus measured or published interactions between them. Baits are shown as large red squares. Solid lines represent specific interactions identified by AP-MS/MS analysis, grey lines represent published protein-protein interactions from IntAct and CORUM databases. Up- or downregulation at the proteome level is marked with filled circles (hNPC: up – red, down – dark blue; SK-N-BE2: up – orange, down – light blue). Phosphorylation changes in SK-N-BE2 are presented as red (up) or blue (down) circle borders.

References

1 Miner, J. J. & Diamond, M. S. Zika Virus Pathogenesis and Tissue Tropism. *Cell host & microbe* **21**, 134-142, doi:10.1016/j.chom.2017.01.004 (2017).

2 Acosta, E. G., Kumar, A. & Bartenschlager, R. Revisiting dengue virus-host cell interaction: new insights into molecular and cellular virology. *Advances in virus research* **88**, 1-109, doi:10.1016/B978-0-12-800098-4.00001-5 (2014).

3 Shan, C. *et al.* An Infectious cDNA Clone of Zika Virus to Study Viral Virulence, Mosquito Transmission, and Antiviral Inhibitors. *Cell host & microbe* **19**, 891-900, doi:10.1016/j.chom.2016.05.004 (2016).

4 Chatel-Chaix, L. *et al.* Dengue Virus Perturbs Mitochondrial Morphodynamics to Dampen Innate Immune Responses. *Cell host & microbe* **20**, 342-356, doi:10.1016/j.chom.2016.07.008 (2016).

5 Balinsky, C. A. *et al.* Nucleolin interacts with the dengue virus capsid protein and plays a role in formation of infectious virus particles. *Journal of virology* **87**, 13094-13106, doi:10.1128/JVI.00704-13 (2013).

6 Colpitts, T. M., Barthel, S., Wang, P. & Fikrig, E. Dengue virus capsid protein binds core histones and inhibits nucleosome formation in human liver cells. *PloS one* **6**, e24365, doi:10.1371/journal.pone.0024365 (2011).

7 You, J. *et al.* Flavivirus Infection Impairs Peroxisome Biogenesis and Early Antiviral Signaling. *Journal of virology* **89**, 12349-12361, doi:10.1128/JVI.01365-15 (2015).

8 Slomnicki, L. P. *et al.* Nucleolar Enrichment of Brain Proteins with Critical Roles in Human Neurodevelopment. *Molecular & cellular proteomics : MCP* **15**, 2055-2075, doi:10.1074/mcp.M115.051920 (2016).

9 Li, H. *et al.* Ly-1 antibody reactive clone is an important nucleolar protein for control of self-renewal and differentiation in embryonic stem cells. *Stem cells* **27**, 1244-1254, doi:10.1002/stem.55 (2009).

10 Jung, M. Y., Lorenz, L. & Richter, J. D. Translational control by neuroguidin, a eukaryotic initiation factor 4E and CPEB binding protein. *Molecular and cellular biology* **26**, 4277-4287, doi:10.1128/MCB.02470-05 (2006).

11 Liang, Q. *et al.* Zika Virus NS4A and NS4B Proteins Deregulate Akt-mTOR Signaling in Human Fetal Neural Stem Cells to Inhibit Neurogenesis and Induce Autophagy. *Cell stem cell* **19**, 663-671, doi:10.1016/j.stem.2016.07.019 (2016).

12 Radke, J., Stenzel, W. & Goebel, H. H. Human NCL Neuropathology. *Biochimica et biophysica acta* **1852**, 2262-2266, doi:10.1016/j.bbadis.2015.05.007 (2015).

13 Aravantinou-Fatorou, K. *et al.* CEND1 and NEUROGENIN2 Reprogram Mouse Astrocytes and Embryonic Fibroblasts to Induced Neural Precursors and Differentiated Neurons. *Stem cell reports* **5**, 405-418, doi:10.1016/j.stemcr.2015.07.012 (2015).

14 Ochrietor, J. D. & Linser, P. J. 5A11/Basigin gene products are necessary for proper maturation and function of the retina. *Developmental neuroscience* **26**, 380-387, doi:10.1159/000082280 (2004).

15 Politis, P. K. *et al.* BM88/CEND1 coordinates cell cycle exit and differentiation of neuronal precursors. *Proceedings of the National Academy of Sciences of the United States of America* **104**, 17861-17866, doi:10.1073/pnas.0610973104 (2007).

16 Gehman, L. T. *et al.* The splicing regulator Rbfox2 is required for both cerebellar development and mature motor function. *Genes & development* **26**, 445-460, doi:10.1101/gad.182477.111 (2012).

17 Bi, J. *et al.* Basigin null mutant male mice are sterile and exhibit impaired interactions between germ cells and Sertoli cells. *Developmental biology* **380**, 145-156, doi:10.1016/j.ydbio.2013.05.023 (2013).
18 Tarlungeanu, D. C. *et al.* Impaired Amino Acid Transport at the Blood Brain Barrier Is a Cause of Autism Spectrum Disorder. *Cell* **167**, 1481-1494 e1418, doi:10.1016/j.cell.2016.11.013 (2016).
19 Souza, B. S. *et al.* Zika virus infection induces mitosis abnormalities and apoptotic cell death of human neural progenitor cells. *Scientific reports* **6**, 39775, doi:10.1038/srep39775 (2016).
20 Zhang, F. *et al.* Molecular signatures associated with ZIKV exposure in human cortical neural progenitors. *Nucleic acids research* **44**, 8610-8620, doi:10.1093/nar/gkw765 (2016).
21 Tang, H. *et al.* Zika Virus Infects Human Cortical Neural Progenitors and Attenuates Their Growth. *Cell stem cell* **18**, 587-590, doi:10.1016/j.stem.2016.02.016 (2016).
22 Watanabe, K. *et al.* A ROCK inhibitor permits survival of dissociated human embryonic stem cells. *Nature biotechnology* **25**, 681-686, doi:10.1038/nbt1310 (2007).
23 Li, X., Long, J., He, T., Belshaw, R. & Scott, J. Integrated genomic approaches identify major pathways and upstream regulators in late onset Alzheimer's disease. *Scientific reports* **5**, 12393, doi:10.1038/srep12393 (2015).
24 O'Rourke, J. G. *et al.* SUMO-2 and PIAS1 modulate insoluble mutant huntingtin protein accumulation. *Cell reports* **4**, 362-375, doi:10.1016/j.celrep.2013.06.034 (2013).
25 Soderholm, S. *et al.* Phosphoproteomics to Characterize Host Response During Influenza A Virus Infection of Human Macrophages. *Molecular & cellular proteomics : MCP* **15**, 3203-3219, doi:10.1074/mcp.M116.057984 (2016).
26 Wojcechowskyj, J. A. *et al.* Quantitative phosphoproteomics reveals extensive cellular reprogramming during HIV-1 entry. *Cell host & microbe* **13**, 613-623, doi:10.1016/j.chom.2013.04.011 (2013).
27 Stahl, J. A. *et al.* Phosphoproteomic analyses reveal signaling pathways that facilitate lytic gammaherpesvirus replication. *PLoS pathogens* **9**, e1003583, doi:10.1371/journal.ppat.1003583 (2013).
28 Ohman, T. *et al.* Phosphoproteome characterization reveals that Sendai virus infection activates mTOR signaling in human epithelial cells. *Proteomics* **15**, 2087-2097, doi:10.1002/pmic.201400586 (2015).
29 Zhang, H. *et al.* Quantitative Label-Free Phosphoproteomics Reveals Differentially Regulated Protein Phosphorylation Involved in West Nile Virus-Induced Host Inflammatory Response. *Journal of proteome research* **14**, 5157-5168, doi:10.1021/acs.jproteome.5b00424 (2015).
30 Humphrey, S. J., Azimifar, S. B. & Mann, M. High-throughput phosphoproteomics reveals in vivo insulin signaling dynamics. *Nature biotechnology* **33**, 990-995, doi:10.1038/nbt.3327 (2015).
31 Cao, B., Parnell, L. A., Diamond, M. S. & Mysorekar, I. U. Inhibition of autophagy limits vertical transmission of Zika virus in pregnant mice. *The Journal of experimental medicine* **214**, 2303-2313, doi:10.1084/jem.20170957 (2017).
32 Rhim, J. H. *et al.* Cell type-dependent Erk-Akt pathway crosstalk regulates the proliferation of fetal neural progenitor cells. *Scientific reports* **6**, 26547, doi:10.1038/srep26547 (2016).
33 Ghouzzi, V. E. *et al.* ZIKA virus elicits P53 activation and genotoxic stress in human neural progenitors similar to mutations involved in severe forms of genetic microcephaly and p53. *Cell death & disease* **7**, e2440, doi:10.1038/cddis.2016.266 (2016).
34 Yamashita, N. *et al.* Phosphorylation of CRMP2 (collapsin response mediator protein 2) is involved in proper dendritic field organization. *The Journal of neuroscience : the official journal of the Society for Neuroscience* **32**, 1360-1365, doi:10.1523/JNEUROSCI.5563-11.2012 (2012).

35 Li, H., Chen, G., Zhou, B. & Duan, S. Actin filament assembly by myristoylated alanine-rich C kinase substrate-phosphatidylinositol-4,5-diphosphate signaling is critical for dendrite branching. *Molecular biology of the cell* **19**, 4804-4813, doi:10.1091/mbc.E08-03-0294 (2008).
36 Morooka, T. & Nishida, E. Requirement of p38 mitogen-activated protein kinase for neuronal differentiation in PC12 cells. *The Journal of biological chemistry* **273**, 24285-24288 (1998).
37 Xu, X. H. *et al.* MARCKS regulates membrane targeting of Rab10 vesicles to promote axon development. *Cell research* **24**, 576-594, doi:10.1038/cr.2014.33 (2014).
38 Morimura, R., Nozawa, K., Tanaka, H. & Ohshima, T. Phosphorylation of Dpsyl2 (CRMP2) and Dpsyl3 (CRMP4) is required for positioning of caudal primary motor neurons in the zebrafish spinal cord. *Developmental neurobiology* **73**, 911-920, doi:10.1002/dneu.22117 (2013).
39 Marceau, C. D. *et al.* Genetic dissection of Flaviviridae host factors through genome-scale CRISPR screens. *Nature* **535**, 159-163, doi:10.1038/nature18631 (2016).
40 Savidis, G. *et al.* Identification of Zika Virus and Dengue Virus Dependency Factors using Functional Genomics. *Cell reports* **16**, 232-246, doi:10.1016/j.celrep.2016.06.028 (2016).
41 Chavali, P. L. *et al.* Neurodevelopmental protein Musashi-1 interacts with the Zika genome and promotes viral replication. *Science* **357**, 83-88, doi:10.1126/science.aam9243 (2017).
42 Barrows, N. J. *et al.* A Screen of FDA-Approved Drugs for Inhibitors of Zika Virus Infection. *Cell host & microbe* **20**, 259-270, doi:10.1016/j.chom.2016.07.004 (2016).
43 Shao, Q. *et al.* The African Zika virus MR-766 is more virulent and causes more severe brain damage than current Asian lineage and dengue virus. *Development* **144**, 4114-4124, doi:10.1242/dev.156752 (2017).
44 Swistowski, A. *et al.* Xeno-free defined conditions for culture of human embryonic stem cells, neural stem cells and dopaminergic neurons derived from them. *PloS one* **4**, e6233, doi:10.1371/journal.pone.0006233 (2009).
45 Paul, D., Bartenschlager, R. & McCormick, C. The predominant species of nonstructural protein 4B in hepatitis C virus-replicating cells is not palmitoylated. *The Journal of general virology* **96**, 1696-1701, doi:10.1099/vir.0.000111 (2015).
46 Rappsilber, J., Mann, M. & Ishihama, Y. Protocol for micro-purification, enrichment, pre-fractionation and storage of peptides for proteomics using StageTips. *Nature protocols* **2**, 1896-1906, doi:10.1038/nprot.2007.261 (2007).
47 Steger, M. *et al.* Phosphoproteomics reveals that Parkinson's disease kinase LRRK2 regulates a subset of Rab GTPases. *eLife* **5**, doi:10.7554/eLife.12813 (2016).
48 Scaturro, P., Cortese, M., Chatel-Chaix, L., Fischl, W. & Bartenschlager, R. Dengue Virus Non-structural Protein 1 Modulates Infectious Particle Production via Interaction with the Structural Proteins. *PLoS pathogens* **11**, e1005277, doi:10.1371/journal.ppat.1005277 (2015).
49 Gebhardt, A. *et al.* mRNA export through an additional cap-binding complex consisting of NCBP1 and NCBP3. *Nature communications* **6**, 8192, doi:10.1038/ncomms9192 (2015).
50 Hubner, N. C. *et al.* Quantitative proteomics combined with BAC TransgeneOmics reveals in vivo protein interactions. *The Journal of cell biology* **189**, 739-754, doi:10.1083/jcb.200911091 (2010).
51 Hornbeck, P. V. *et al.* PhosphoSitePlus, 2014: mutations, PTMs and recalibrations. *Nucleic acids research* **43**, D512-520, doi:10.1093/nar/gku1267 (2015).
52 Schindelin, J. *et al.* Fiji: an open-source platform for biological-image analysis. *Nature methods* **9**, 676-682, doi:10.1038/nmeth.2019 (2012).